ACTIVE SUSPENSION CO-DESIGN FOR LATERAL STABILITY OF RAIL VEHICLES

BY

MADHAV ARORA

THESIS

Submitted in partial fulfillment of the requirements
for the degree of Master of Science in Industrial Engineering
in the Graduate College of the
University of Illinois at Urbana-Champaign, 2017

Urbana, Illinois

Adviser:

Assistant Professor James T. Allison

Abstract

Railroad transportation is one of the most cost-effective and energy-efficient modes of land transportation. With an eye toward improving these efficiencies, many efforts have focused on developing high speed railways. Traditionally railways have utilized passive suspension systems, but maintaining dynamic stability at higher speeds demands enhancements to existing rail vehicle suspensions. One strategy to improve dynamic performance is to incorporate active or semi-active elements, such as force actuators or variable dampers, within the suspension system. Modern day road and rail vehicles often utilize such actively-controlled suspensions to improve stability, ride comfort and ride quality at high speeds. The dynamic performance of such mechatronically-controlled suspension systems is related closely to the congruence of the design of passive elements in conjunction with the chosen control system strategy. Historically, design of controlled dynamic systems has followed a sequential process (mechanical design followed by control design). In the field of mechatronics, engineers typically use design rules or heuristics that help account for design coupling, but cannot produce system-optimal designs. Passive elements are optimally designed first, followed by the addition of controllers for system performance improvements. New integrated design strategies are required to realize the full potential of such advanced complex dynamic systems and to capitalize on design coupling.

This thesis aims to explore and apply a recently developed synergistic approach to design of controlled dynamic systems, called co-design. Theoretical models of existing partitioned, optimization-based design methods are compared to this combined active and passive system design strategy. Parameters for a reduced and a full-scale rail vehicle model are then designed using the developed optimal design formulations. Different control techniques within the co-design framework are tested and compared. Typically feedback controllers are required for actual implementation of control

strategies. Early-stage co-design strategies are normally based on open-loop control, therefore, are limited for functional implementation. However, co-design methods provide designers with better knowledge about the true performance limits of dynamic systems, help them make more informed design decisions, and provide a foundation for development of implementable feedback control systems. The results obtained in this thesis show significant improvements achieved by co-design strategies over passive system design and sequential design approaches. The results also demonstrate the potential of this framework in helping systematic selection of optimal plant design variables, controller architecture, and implementable control techniques. Future work includes designing practical feedback controllers built upon results from co-design strategies for rail vehicles using non-linear vehicle models to provide a complete active rail suspension solution.

To my parents, my brother and Hugo.

Acknowledgments

I wish to express my sincere appreciation and gratitude toward Professor James T. Allison for his invaluable guidance and motivation throughout this thesis work. In addition, I would like thank the Engineering System Design Lab (ESDL) team, especially Anand Deshmukh, Daniel Herber, Yong-Hoon Lee, Danny Lohan, and Albert Patterson for always answering my innumerous questions and making me a true design researcher.

I would also like to thank Faaiza and Jeb for trudging through the countless days and nights of hard work together, and motivating me to keep doing better.

Last but not the least, I am immensely proud to be a part of the Department of Industrial & Enterprise Systems Engineering, and grateful to Professor Allison for the continued moral and financial support without which this work would not have come to fruition.

Table of Contents

List of Tables

List of Figures

Nomenclature

λ	Effective wheel conicity
σ	Wheelset Roll Coeffecient
ζ	Creep Constant
a	Half of wheelset contact distance
b	Half of Wheelbase
d_s	Half of secondary spring spacing
d_p	Half of primary spring spacing
f_{11}	Lateral Creep Coefficient
f_{12}	Lateral Spin Creep Coeffecient
f_{22}	Spin Creep Coeffecient
f_{33}	Longitudinal Creep Coeffecient
h_{cs}	Vertical distance from car body c.o.g. to secondary spring
h_{tp}	Vertical distance from truck c.o.g. to primary springs
h_{ts}	Vertical distance from truck c.o.g. to secondary springs
I_{cx}	Roll Moment of Inertia of car body
I_{cy}	Pitch Moment of Inertia of car body
I_{cz}	Yaw Moment of Inertia of car body
I_{tx}	Roll Moment of Inertia of truck

I_{ty}	Pitch Moment of Inertia of truck
I_{wx}	Roll Moment of Inertia of wheelset
I_{wy}	Pitch Moment of Inertia of car body
I_{wz}	Yaw Moment of Inertia of car body
l_c	Total lenth of car body
l_s	Half of truck center pin spacing
m_c	Mass of car body
m_t	Mass of truck
m_w	Mass of wheelset
r_0	Cenetered wheel rolling radius
W	Weight of car body

Chapter 1

Introduction

Rail vehicles are complex, dynamic systems. Modern day rail cars utilize elaborate mechatronics to improve performance, comfort, and reliability. Conventional design approaches for such advanced rail vehicle suspensions often overlook the symbiosis between passive and active elements of design. There is a need to reassess existing methods and scrutinize newer synergistic design strategies.

1.1 Rail Vehicle Design

With the recent introduction of high-speed rail in countries around the world such as France, Spain, Japan, and China, improving the dynamic performance of rail vehicles presently holds paramount importance. Performance factors including ride quality, ride comfort, and dynamic stability of rail-cars are closely related to the optimization of the underlying suspension systems. Passive suspension systems, currently ubiquitous in rail vehicles, have limited dynamic capabilities. Actively-controlled suspensions can be used to improve conflicting objectives simultaneously, such as curve negotiability and tangent track speeds. Safety of railway passengers and operational reliability of high speed trains can also be improved significantly by minimizing unwanted disturbances, such as hunting. Figure 1.1 shows the Japanese Shikansen 500, one of the earliest in-service passenger railcars to adopt lateral semi-active suspensions to improve dynamic stability, ride comfort and minimize effects of hunting at high speeds.

Researchers have developed and validated detailed dynamic models with passive suspension elements with varying degrees of complexity. Garg and Dukkipati [5] developed extensive linear and non-linear models of passenger and freight railway vehicles on both tangent and curved tracks using various

Table 1.1: In-service high speed trains with active suspensions and associated control strategies [1]

Train, Country	Active Control Technique and Strategy
Pendolino, Spain and Britain	Tilt and Centering; Hold-Off Device
Shinkansen Series 700, Japan	Semi-active lateral suspension; Sky-Hook Damping
Shinkansen Series E, Japan	Active pneumatic actuators; H_∞ control
Shinkansen Fastech 360, Japan	Semi-active; electro-magnetic actuators

deterministic and random track inputs. Cheng et al. [6] derived 20-DOF (degree-of-freedom), 14-DOF, and 6-DOF linear vehicle dynamics models, and evaluated critical hunting speed via heuristic non-linear and linear creep models on curved tracks. Graa et al. [7] proposed a 38-DOF model and validated it using both experimental data and results produced by more complex models from the literature. Hirotsu et al. [8] derived and formulated a 31-DOF model, and found that yaw dampers had a large effect on improving the lateral vehicle stability, especially in suppressing divergent hunting at higher vehicle speeds. This is discussed in further detail in Chapters 3 and 4.

Active suspension systems for rail vehicles, while not a recent technological development [9], have found limited adoption in the rail industry. The primary impediment is cost of mechatronic systems, as well as the significant service life of typical rail-cars (30-70 years) [10]. Goodall et al. [11] noted the ever-increasing importance of mechatronic solutions to vehicle designs, but acknowledged that the rail industry is falling behind the aircraft and automotive industries in their implementation. As the rail industry seeks to compete with other means of transportation, increased speed and reliability are important factors for future economic success. Active suspension systems provide a gateway to achieve these goals by providing advanced controllability and dynamic performance that cannot be attained by passive systems.

A number of control applications for dynamic railway systems have been investigated by researchers. Orvnäs [1] reviewed existing theoretical and practical concepts of active systems and categorized them into two approaches:

- Active suspensions to improve stability and guidance
- Active suspensions to improve ride quality

Figure 1.1: Shinkansen 500 series train, Japan, one of the earliest examples with semi-active lateral suspensions to improve ride comfort [2]

The former deals with the idea of active elements in the primary suspension. The latter employs active secondary suspensions, usually in the lateral and yaw axes and/or for tilting technologies, to enhance passenger ride comfort. Car-body tilting, which uses mechatronic systems to induce an inward roll at curves to reduce centrifugal forces felt by the passengers, has been fairly well-established in current railway systems. Although successfully implemented, tilting trains have been found to cause motion sickness in passengers [12, 13], hence stimulating the need to investigate other possible active technologies.

To actualize an efficient actively-controlled suspension, appropriate actuators must be selected and designed to be governed by suitable control algorithms. Different actuator types include electro-mechanical, electro-magnetic, and hydraulic. These actuators can produce arbitrary force trajectories within limits, but often have prohibitively high power requirements that hinder their widespread use in practice [3]. Another class of actuators has much lower power requirements. Adjustable dampers enable precise control over energy extraction from a suspension system, but do not inject energy into the suspension. As a result, suspensions with adaptive dampers are often called semi-active suspensions. Figure 1.2 illustrates the different suspension strategies investigated for use as secondary suspension systems in rail vehicles.

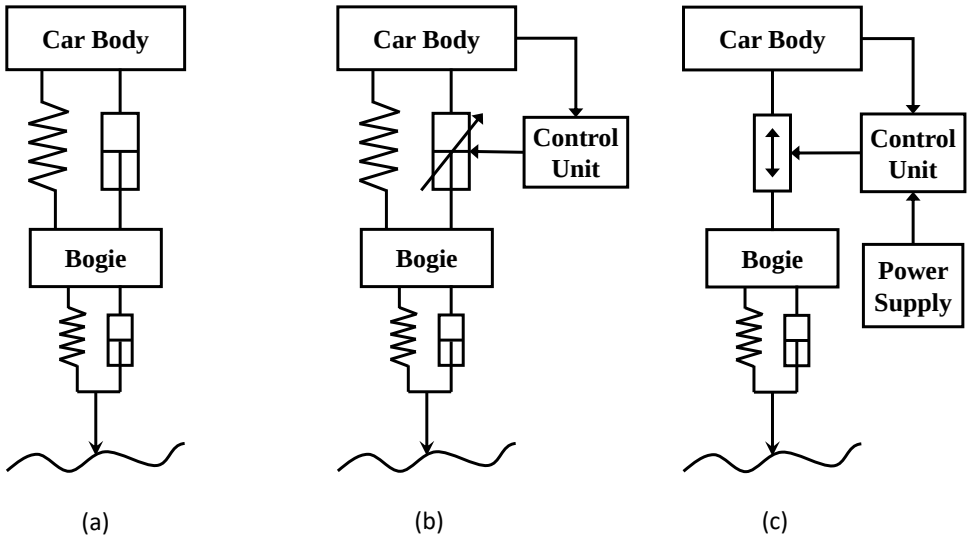

Figure 1.2: Illustration of different secondary suspension strategies for rail vehicles: (a) Passive, (b) Semi-active, and (c) Fully-active [1, 3]

One type of adaptive damper uses electro/magneto-rheological (ER/MR) fluids that are capable of adjustable damping characteristics through the controlled application of electrical current or potential difference. ER fluids are excited by an applied electric field requiring thousands of volts for operation, which leads to safety and packaging concerns for designers and users. In contrast, MR fluids are excited by a magnetic field, which requires only a low voltage source [14]. MR dampers are also relatively inexpensive, and consume very small amounts of energy to control the magnetic field [1]. Du et al. [15] found that semi-active suspensions with MR dampers can achieve performance that is comparable to that of active suspensions, with near-zero power consumption, and are inherently BIBO (Bounded-Input Bounded-Output) stable. The strength of the applied (controlled) magnetic/electric field significantly influences the viscosity of the fluid inside the damper, thereby changing its inherent damping characteristics. The success of MR dampers in semi-active vehicle suspension applications is determined primarily by the accurate modeling of the MR dampers, and the selection of an appropriate control strategy [15]. Modeling and control of MR Dampers is discussed in further detail in Chapter 2.

Semi-active suspensions for rail vehicles using MR dampers have been subject to fairly limited research. One of the widely-adopted control strategies

is Sky-hook damping, which damps the system relative to a fictive sky reference point. Although significant ride quality improvements were found compared to passive systems, the strategy struggled to provide the same level enhancements during curve negotiation and special track conditions [1]. Several researchers have explored optimal control strategies such as Linear Quadratic Gaussian (LQG) control laws with semi-active suspensions. He [16] used multidisciplinary optimization of combined mechanical and control systems based on LQG and Kalman Filter Algorithms to optimize quarter-vehicle (2-DOF) and half-vehicle model suspensions. Wang and Liao [17, 18] created a full-scale model of a railway vehicle integrated with semi-active controlled MR fluid dampers in the lateral secondary suspension system based on their earlier work that demonstrated the feasibility of using MR Dampers for rail purposes [19]. They found that under periodic track irregularities, the semi-active suspension system can attenuate the lateral, yaw, and roll accelerations of the car body significantly (approximately 70%) relative to the passive suspension system. More recent work involves a hardware-in-the-loop simulation (HILS) of MR dampers to test active lateral suspensions [20], linear-quadratic regulator (LQR), and proportional-integral-derivative (PID)-LQR approaches to identify the PID gains needed to improve passenger comfort [7, 21, 22], and semi-active strategies with non-linear passive suspension systems [23].

A brief review of the existing literature adequately affirms the feasibility of using MR fluid dampers for semi-active suspensions to improve lateral stability and comfort of rail vehicles, and further motivates the need to identify and examine robust optimal design and control strategies that help explore tradeoffs and the limits of the overall system performance.

1.2 Dynamic System Design

Designing is a complex decision-making process which is often based on existing design rules, principles, and sequential procedures [24]. Mathematical optimization is the process of maximizing or minimizing one or more objective functions, possibly with constraints, by adjusting a set of variable values that influence both the objectives and the design constraints [25]. Thus, optimal design involves accurate mathematical modeling, choosing an ap-

propriate design objective, choosing the set of design variables, identifying design constraints (time, resources, physical limitations, failure modes, etc.), identifying a suitable solution method, and then solving for the best design alternative.

Active dynamic systems are inherently multi-disciplinary. Established Multidisciplinary Design Optimization (MDO) formulations largely are based on static system analysis or black-box simulations, and often do not address system dynamics explicitly [26]. As a result, the nuances of dynamic behavior are implicitly deemphasized, the special structure of dynamic design problems cannot be exploited, and thus optimal design of controlled dynamic systems becomes a challenging prospect using standard MDO methods. Simulations of such systems are usually computationally expensive, thus making optimizations based on direct simulation often impractical [27].

Allison and Herber [26] defined multidisciplinary dynamic system design optimization (MDSDO) as a branch of MDO that deals with systems where the evolution of system state through time is a critical element of performance, and where the unique properties of dynamic systems are exploited to improve system performance and yield efficient problem solutions.

Historically, design of active dynamic systems has been carried out sequentially. The physical design is explored, optimized, and fixed, following which a controller is added to the system that can then be optimized. Integrating the physical (plant) and control aspects of dynamic system design has the ability to probe performance gains which may be indiscoverable with the sequential design processes. The preferred approach simultaneously considers the plant and control design, and is often referred to as co-design [28].

Co-design leverages the use of existing indirect and direct design methods used in solving optimal design problems, and integrates physical (plant) design variables, typically using either a single simultaneous or bi-level nested optimization formulation. This allows the exploitation of the synergy between both disciplines and the identification of system-optimal solutions [27]. Figure 1.3 illustrates the various strategies discussed in this thesis for solving dynamic system design problems.

Conventional optimal control methods take an 'optimize-then-discretize' approach, where optimality conditions are applied to generate a boundary value problem that in special cases leads to a closed-form solution. A class of direct methods known Direct Transcription (DT) uses a powerful 'discretize-

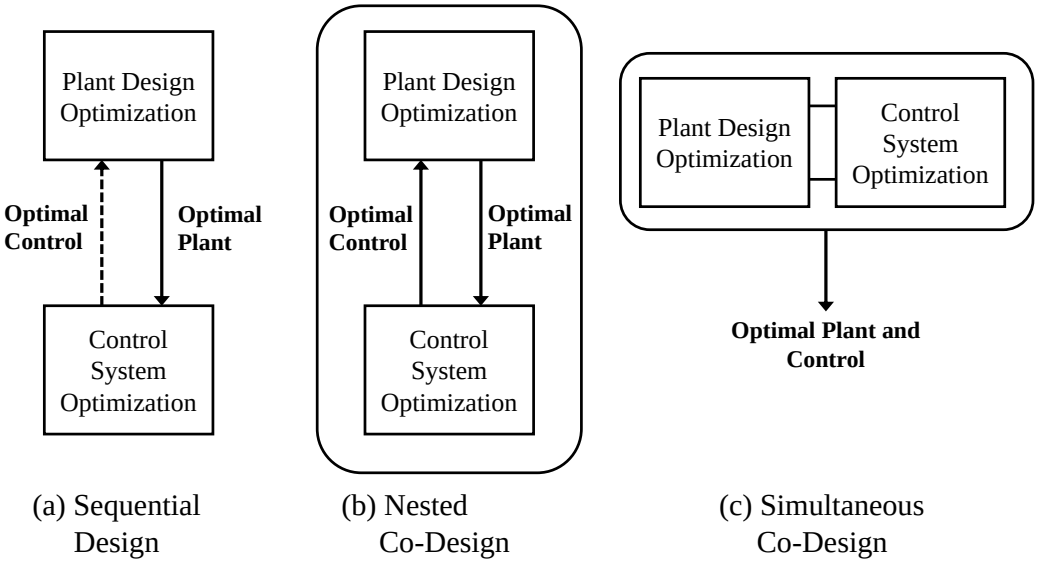

(a) Sequential Design (b) Nested Co-Design (c) Simultaneous Co-Design

Figure 1.3: Strategies to Solve Dynamic System Design Problems

then-optimize' approach. An infinite-dimensional optimal control problem is transcribed to a finite-dimensional NLP [29]. DT-based co-design supports a balanced approach in which plant and control are both given thorough treatment, enabling engineers to construct a formulation that supports improving overall system utility [26]. DT has been used to solve open-loop optimal control problems and dynamic system co-design problems with great success [3, 26, 28, 30, 31].

1.3 Thesis Overview

This thesis aims to leverage the state-of-the-art in integrated optimal physical and control system design to explore the performance limits of active and semi-active suspensions in rail vehicles. A number of different suspension configurations are modeled and optimized, and the results are discussed.

Chapter 2 reviews dynamic system design optimization and co-design techniques. Chapter 3 discusses the modeling of rail vehicle dynamics, modeling of MR dampers, state-space modeling, and optimization setup. Chapter 4 presents the numerical studies and results based on different models, solution techniques, and suspension configurations. Chapter 5 concludes and summarizes the findings.

Chapter 2

Co-Design of Dynamic Systems

2.1 Design Optimization

In mathematical optimization, the maximum or minimum value of a function is sought, possibly within constraints on the function input variables. Optimization algorithms applied to engineering design are methodical processes that involve changing input variable values (design variables) to improve objective function values within the feasible design space (defined by the design constraints) [25]. Optimization-based engineering design is a well-established design strategy. Papalambros [32] broke down the design optimization procedure into four primary stages:

- Selection of a set of variables to describe the design alternatives
- Selection of an objective (criterion), expressed in terms of the design variables
- Determination of a set of constraints, expressed in terms of the design variables
- Determination of a set of values for the design variables, which minimize (or maximize) the objective, while satisfying all the constraints

An optimization-based approach in engineering design is used to identify the most optimal set of solutions for an existing, well-formulated problem. Typically set up in the negative null form, a general NLP can be expressed as:

$$\min_{\mathbf{x}} \quad f(\mathbf{x}) \tag{2.1a}$$

$$\text{subject to:} \quad \mathbf{h}(\mathbf{x}) = 0 \tag{2.1b}$$

$$\mathbf{g}(\mathbf{x}) \leq 0 \tag{2.1c}$$

where $\mathbf{x}$ is the vector of optimization variables, $f(\mathbf{x})$, is the objective function, and $\mathbf{h}(\mathbf{x})$ and $\mathbf{g}(\mathbf{x})$ represent the vector-valued equality and inequality constraints, respectively.

Engineering design problems can often be posed naturally as constrained optimization problems [33]. Constraints can be based on requirements and physical limitations (e.g., stress, temperature, packaging, etc.). Design decision variables are given as inputs to the system with suitable starting points and lower and upper bounds. Design variables should be independent. Objective (or "cost") functions may be a single metric, multiple objectives, or a weighted aggregate of multiple objectives.

2.2 Design of Dynamic Systems

Dynamic systems, being time-dependent systems, require more involved design formulations. Optimal design of dynamic systems must involve a comprehensive treatment of system dynamics. Conventional physical design formulations incorporate simplified dynamics, as shown in Eqn. (2.1a). Dynamic system models often incorporate realistic dynamics in state-space form:

$$\dot{\boldsymbol{\xi}}(t) = \mathbf{f}(\boldsymbol{\xi}(t), \mathbf{x_p}, t) \tag{2.2}$$

where $\boldsymbol{\xi}(t)$ and $\dot{\boldsymbol{\xi}}(t)$ are the state trajectories and their derivatives, respectively, and $\mathbf{x_p}$ is the vector of physical system design (plant) variables. Plant design variables may include suspension stiffness coefficients, damping coefficients, geometric parameters, etc. Although such models require advanced development effort, they allow complex formulations with enhanced flexibility for optimization [26].

For a controlled linear time-invariant (LTI) system, the same derivative function can be written as:

$$\dot{\boldsymbol{\xi}}(t) = \mathbf{f}(\boldsymbol{\xi}(t), \mathbf{u}(t), \mathbf{x_p}, t) = \mathbf{A}\boldsymbol{\xi}(t) + \mathbf{B}\mathbf{u}(t) \tag{2.3}$$

where $\mathbf{A}$ is the state matrix and $\mathbf{B}$ is the input matrix. The state trajectories for general state-space systems can be obtained using numerical simulation. Closed-form solutions exist for LTI systems. State-space models can be generated using established modeling techniques, such as bond graph modeling.

State-space modeling for rail vehicle suspensions will be discussed further in Chapter 3.

2.2.1 Sequential Design

Typically in design practice, sequential design approaches are used. The passive physical system is designed and optimized first, and then the control variables are designed based on the optimal passive solution obtained. Consider the following optimal physical system design model:

$$\min_{\mathbf{x_p}} \quad \psi(\boldsymbol{\xi}(t), \mathbf{x_p}, t) \tag{2.4a}$$

$$\text{subject to:} \quad \mathbf{g_p}(\boldsymbol{\xi}(t), \mathbf{x_p}) \leq \mathbf{0}, \tag{2.4b}$$

$$\dot{\boldsymbol{\xi}}(t) - \mathbf{f}(\boldsymbol{\xi}(t), \mathbf{x_p}, t) = \mathbf{0} \tag{2.4c}$$

where the cost function $\psi(\cdot)$ is optimized with respect to the plant design variables $\mathbf{x_p}$, $\boldsymbol{\xi}(t)$ are the state trajectories as defined in Eqn. (2.2), and $\mathbf{g_p}(\cdot)$ define physical system constraints such as stress, deflection, packaging, or other geometric requirements. This formulation includes both the state trajectories along with physical design variables, accounting for system dynamics directly instead of assuming quasi-static behavior. The system model must support dynamic behavior prediction with changing design variable values. This property is often not present in dynamic system models developed for control system design.

Solutions to such problems can be obtained using inner-loop simulations, surrogate modeling, and other indirect and direct methods of problem solution. The solution to Prob. (2.4) will provide the optimal plant design vector $\mathbf{x_{p_*}}$, which is then used as a fixed parameter when solving the subsequent optimal control design problem:

$$\min_{\mathbf{u}(t)} \quad \psi(\boldsymbol{\xi}(t), \mathbf{u}(t), \mathbf{x_{p_*}}) \tag{2.5a}$$

$$\text{subject to:} \quad \mathbf{g_p}(\boldsymbol{\xi}(t), \mathbf{x_{p_*}}) \leq \mathbf{0}, \tag{2.5b}$$

$$\dot{\boldsymbol{\xi}}(t) - \mathbf{f}(\boldsymbol{\xi}(t), \mathbf{u}(t), \mathbf{x_{p_*}}, t) = \mathbf{0} \tag{2.5c}$$

where $\mathbf{u}(t)$ are the time dependent control variable trajectories, and $\mathbf{x_{p_*}}$ is the optimal physical system design determined during plant design optimization.

The solution to Prob. (2.5) may provide a feasible design, but does not fully incorporate the synergy between the plant design variables, state trajectories, and control design vector. The design space exploration is limited due to the sequential nature of the approach, as the control solutions are explored for a single optimal physical design. As actively controlled systems become more complex and performance requirements more stringent, sequential system design may fall short, motivating the use of more integrated design methods that can account fully for plant-control design coupling [26].

2.2.2 Open-Loop Optimal Control

Open loop optimal control or optimal control system design (OCSD) [28] is a well-established subject of research. Applications for optimal control include robotic manipulations, aerospace controller design, and drone manipulator designs. An optimal control formulation is infinite-dimensional since the control trajectories, which are the optimization variables, vary with time. One possible OCSD formulation is:

$$\min_{\mathbf{u}(t)} \quad \psi = \int_{t_0}^{t_f} \mathcal{L}(\boldsymbol{\xi}(t), \mathbf{u}(t), t)dt + \mathcal{M}(\boldsymbol{\xi}(t_0), \boldsymbol{\xi}(t_f), t_0, t_f) \tag{2.6a}$$

$$\text{s.t.} \quad \dot{\boldsymbol{\xi}}(t) - \mathbf{f}(\boldsymbol{\xi}(t), \mathbf{u}(t), t) = \mathbf{0}. \tag{2.6b}$$

$$\mathcal{C}(\boldsymbol{\xi}(t), \mathbf{u}(t), t) \leq \mathbf{0} \tag{2.6c}$$

$$\boldsymbol{\phi}(\boldsymbol{\xi}(t_0), \boldsymbol{\xi}(t_f), t_0, t_f) \leq \mathbf{0} \tag{2.6d}$$

Important problem elements are described below:

Objective function: The objective function in Prob. (2.6) contains two main terms, $\mathcal{L}(\cdot)$, the Lagrange (or running cost) term, and and $\mathcal{M}(\cdot)$, the Mayer term. The Lagrange term is an integral calculated over the finite time horizon, and includes any objective terms that vary with time within the time horizon. The Mayer term includes objectives that depend on only on the initial and final time points, t_0 and t_f. The initial and final time points may also be included as optimization variables in this formulation, for example, if the goal is to minimize the total time required to complete a task. This two-term objective function can be converted into a single-term objective function using the transformations: $\mathcal{L}(\cdot) \rightarrow \mathcal{M}(\cdot)$ or $\mathcal{M}(\cdot) \rightarrow \mathcal{L}(\cdot)$

[28]. The former transformation requires addition of an auxiliary state.

Constraints: There are three types of constraints in the OCSD formulation: 1) dynamic constraints, 2) path constraints, and 3) and boundary constraints. The dynamic constraints ensure that the system satisfies the dynamics as approximated by the state-space equations presented in Prob. (2.3) (e.g., the state trajectories satisfy physics, approximately). Path constraints, $\mathcal{C}(\cdot)$, include most traditional engineering constraints such as stress, power, force, pressure, etc. These constraints must be satisfied at all time points in the time horizon, thereby creating a multi-point boundary value problem (BVP). Path constraints may switch activity multiple times throughout the time horizon. The third type of constraint, represented using $\boldsymbol{\phi}(\cdot)$, are the boundary constraints. These are to be satisfied only at the boundary time points, i.e., at t_0 and t_f.

Control Trajectories: The function-valued control vector $\mathbf{u}(t)$ is optimized to minimize the above objective function, while satisfying dynamic and path constraints. The solution to this problem is a set of control trajectories that optimize the dynamics of a given fixed physical system design.

2.3 Co-Design Strategies

Herber and Allison [34] formalized several co-design formulations, and presented two co-design strategies based on their earlier work [26].

2.3.1 Nested Co-Design

Deshmukh [30] identified that the optimal design of complex, dynamic systems is typically an iterative process involving plant and control design, and involves exploring the strong interdependence between the two aspects. Allison and Herber [35] identified Nested Co-Design as a special case of the Multi-Disciplinary Feasibile (MDF) MDO formulation [36]. A bi-level design methodology incorporating one outer loop and one inner loop can be used to leverage existing OCSD methods for system optimal designs.

Outer Loop The outer loop formulation may be defined as:

$$\begin{array}{ll} \min\limits_{\mathbf{x_p}} & \psi(\mathbf{x_p}) \\ \text{s.t.} & \left.\begin{array}{l} \phi_p(\mathbf{x_p}) \leq \mathbf{0} \\ \mathbf{F}(\mathbf{x_p}) \leq \mathbf{0} \end{array}\right\} \quad \mathbf{g_p}(\mathbf{x_p}) \leq \mathbf{0} \end{array} \tag{2.7}$$

where $\mathbf{x_p}$ is the plant design variable vector, and $\mathbf{g_p}$ is the collection of the outer-loop constraints. Herber and Allison [34] define $\phi_p(\mathbf{x_p})$ as the constraints that depend only on the plant design variables, and $\mathbf{F}(\mathbf{x_p})$ as an additional constraint that may be added to ensure outer-loop feasibility. The outer loop provides a candidate solution, ${\mathbf{x_p}}^\dagger$ rather than an optimal solution, to the inner loop. The inner-loop optimal control problem must be solved for each plant design candidate considered by the outer-loop optimal plant design problem.

Inner Loop The inner-loop problem may be formulated as:

$$\begin{array}{ll} \min\limits_{\mathbf{x_c}} & \psi({\mathbf{x_p}}^\dagger, \mathbf{x_c}) \\ \text{s.t.} & \left.\begin{array}{l} \dot{\boldsymbol{\xi}}(t) - \mathbf{f}(t, \boldsymbol{\xi}(t), {\mathbf{x_p}}^\dagger, \mathbf{x_c}) = \mathbf{0} \\ \mathcal{C}(t, \boldsymbol{\xi}(t), {\mathbf{x_p}}^\dagger, \mathbf{x_c}) \leq \mathbf{0} \\ \boldsymbol{\phi_c}(\boldsymbol{\xi}(t_0), \boldsymbol{\xi}(t_f), {\mathbf{x_p}}^\dagger, \mathbf{x_c}) \leq \mathbf{0} \end{array}\right\} \quad \mathbf{g_c}(\mathbf{x_p}, \mathbf{x_c}) \leq \mathbf{0} \end{array} \tag{2.8}$$

where ${\mathbf{x_p}}^\dagger$ is a candidate plant design vector, $\mathbf{x_c}$ is the control design vector (a more general form, previously referred to as $\mathbf{u}(t)$), $\boldsymbol{\phi_c}(\cdot)$ are the constraints on control and state trajectories. $\mathcal{C}(\cdot)$ includes the traditional path constraints, and $\mathbf{g_c}$ is the collection of inner-loop constraints. Note that an equality constraint may be expressed as two inequality constraints.

The inner optimization loop identifies the optimal control for each candidate plant design tested by the outer loop. Thus, in the above formulation, similar to the sequential design approach, the plant design is held fixed during the control design solution. Plant design constraints are imposed in both loops to ensure system-level design feasibility.

2.3.2 Simultaneous Co-Design

The simultaneous co-design problem may be formulated as:

$$\begin{aligned} \min_{\mathbf{x_c},\mathbf{x_p}} \quad & \psi = \int_{t_0}^{t_F} \mathcal{L}(t, \boldsymbol{\xi}(t), \mathbf{x_c}, \mathbf{x_p}) dt + \mathcal{M}(\boldsymbol{\xi}(t_0), \boldsymbol{\xi}(t_f), t_0, t_f, \mathbf{x_c}, \mathbf{x_p}) \\ \text{s.t.} \quad & \dot{\boldsymbol{\xi}}(t) - \mathbf{f}(t, \boldsymbol{\xi}(t), \mathbf{x_c}, \mathbf{x_p}) = \mathbf{0} \\ & \mathcal{C}(t, \boldsymbol{\xi}(t), \mathbf{x_c}, \mathbf{x_p}) \leq \mathbf{0} \\ & \phi(\boldsymbol{\xi}(t_0), \boldsymbol{\xi}(t_f), \mathbf{x_c}, \mathbf{x_p}) \leq \mathbf{0} \end{aligned} \tag{2.9}$$

This formulation includes all the terms from the OCSD formulation with the addition of plant variables, $\mathbf{x_p}$. The above formulation accounts for all dynamic interactions and plant design coupling, and results in a system-optimal design[30]. By leveraging the novel aspects of OCSD, this formulation accurately captures the synergy between plant and control design, and often provides significantly better solutions than conventional dynamic system design methods.

It must be noted that these formulations are based on open-loop optimal control. These strategies are used to produce optimal trajectories for state and control to aid the process of design, and to explore the limits of system performance. More practically, closed loop control is used to design a feedback control. OCSD problems may be solved for finding the gain matrix in a closed loop system, but this solution will only be subset of all possible optimal trajectories. Herber [28] identified that limiting the performance of the system should be a calculated decision, not a modeling convenience, and that the ultimate system performance limits can only be identified when solving the optimal control control problem in an unrestricted way.

2.4 Direct Transcription

Solution methods for the co-design formulations defined in the previous section are identical to solution methods for OCSD. These can be classified as:

- Indirect Methods: Based on Calculus of Variations

- Direct Methods:
  - Sequential Methods: Single Shooting, Multiple Shooting
  - Simultaneous Direct Transcription: Local and Global Collocation

Sequential methods usually produce low-accuracy solutions, and face issues with numerical convergence. They are computationally inefficient in comparison to other direct methods mainly due to their inability to efficiently handle path and boundary constraints [28].

Direct Transcription (DT) parameterizes both state and control trajectories. Feasible dynamics are ensured by adding defect constraints as equality constraints. The optimization algorithm is task both with finding the optimal design, as well as finding state trajectories that satisfy dynamics. The number of optimization variables increases significantly according to the number of time steps and state and control variables.

A DT-based simultaneous co-design problem may be formulated as:

$$\begin{aligned} \min_{\boldsymbol{\Xi},\mathbf{U},\mathbf{x_p}} \quad & \psi(\mathbf{t},\boldsymbol{\Xi},\mathbf{U},\mathbf{x_p}) + \mathcal{M}(\boldsymbol{\xi}[t_0],\boldsymbol{\xi}[t_f],t_0,t_f,\mathbf{x_p}) \\ \text{s.t.} \quad & \zeta(\mathbf{t},\boldsymbol{\Xi},\mathbf{U},\mathbf{x_p}) = \mathbf{0} \\ & \mathcal{C}(\mathbf{t},\boldsymbol{\Xi},\mathbf{U},\mathbf{x_p}) \leq \mathbf{0} \\ & \phi(\boldsymbol{\Xi}[t_0],\boldsymbol{\Xi}[t_f],t_0,t_f,\mathbf{x_p}) \leq \mathbf{0} \end{aligned} \tag{2.10}$$

where $\mathbf{t}$ is the discretized time vector with $n_t + 1$ number of discrete time steps:

$$\mathbf{t} = [t_0, t_1, ...t_{nt}] \tag{2.11}$$

This may also be referred to as a grid or mesh. The mesh may be made of equidistant points, but other spacing strategies such as Legendre-Gauss-Lobatto (LGL) or Legendre-Gauss-Radau (LGR) may be used to improve numerical accuracy.

$\boldsymbol{\Xi}$ represents the matrix of discretized states with size $(n_t+1)\times n_\xi$, where n_ξ is the number of states of the system. $\mathbf{U}$ represents the matrix of discretized control trajectories with size $(n_t + 1) \times n_u$, where n_u is the number of state trajectories. To convert the infinite-dimensional state and control trajectories to discretized finite-dimensional representations, approximation methods are used. Two important types of collocation methods used with DT include:

- Local collocation: Single-step methods (e.g., Runge-Kutta methods)

- Global collocation: Pseudospectral methods

In local methods, low-degree polynomial approximations are used to approximate trajectories, and the problem is divided into a large number of finite elements to achieve sufficient accuracy (i.e., large n_t) [28]. Explicit Runge-Kutta methods are generally unsuitable for stiff equations. Implicit methods are often preferred. Because DT is a simultaneous solution strategy, implicit methods do not add the expense of inner-loop implicit equation solution, and often can improve overall solution efficiency over explicit methods.

A simple explicit first order scheme for state estimation is the forward Euler method, which can be described as:

$$\boldsymbol{\xi}[t_k] \approx \boldsymbol{\xi}[t_{k-1}] + h_k \mathbf{f_d}[t_{k-1}] \tag{2.12}$$

This equation is converted into negative null form to form the defect constraints $\zeta(\cdot)$ in Prob. 2.9. The work presented in this thesis utilizes a trapezoidal scheme, an implicit second-order collocation method. A defect constraint based on trapezoidal collocation at time t_k can be described as:

$$\boldsymbol{\zeta}[t_k] = \boldsymbol{\xi}[t_k] - \boldsymbol{\xi}[t_{k-1}] - \frac{h_k}{2}(\mathbf{f_d}[t_k] + \mathbf{f_d}[t_{k-1}]) \tag{2.13}$$

Other important methods for DT with local collocation include the Hermite-Simpson rule and the classical fourth-order Runge-Kutta method.

Global collocation methods, also known as pseudospectral methods, use a set of global trial functions with orthogonal collocation to estimate state trajectories. They have a higher degree of accuracy compared to local collocation methods, but require more developmental effort. Certain problem features may also lead to preference for single-step methods.

Finally, the Lagrange (integral) term of the objective function can be approximated using quadrature methods. This thesis utilizes a trapezoidal quadrature rule to estimate the objective function:

$$\int_{t_0}^{t_F} \mathcal{L}(t, \boldsymbol{\xi}(t), \mathbf{x_c}, \mathbf{x_p}) dt \approx \frac{t_f - t_0}{n_t} \left(\frac{\mathcal{L}[t_0]}{2} + \sum_{k=1}^{n_t - 1} \mathcal{L}[t_k] + \frac{\mathcal{L}[t_f]}{2} \right) \tag{2.14}$$

Chapter 3

Modeling

This section deals with deriving the equations of motion for rail vehicle dynamics on a tangent track. Track disturbances are modeled based on linear creep theory. Areas for appropriate use of active control are identified. Two models with varying complexity are then formulated as state-space models for use with co-design studies.

The weight of a rail vehicle's car body is transmitted to rails by components called the rail bogies. A bogie is a chassis or framework carrying multiple wheel-axle sets attached to a vehicle, thus serving as a modular subassembly of wheels and axles [5]. A typical rail vehicle consists of two suspension levels. The primary suspension connects the wheelsets to the rail trucks (or bogies), and the secondary suspension connects the rail trucks to the car body. The car body of a rail vehicle houses the passengers, structures, and equipment. The comfort of a passenger traveling on a train is determined by the response of these primary and secondary suspension systems to track disturbances.

Since the rail vehicle is assumed to make constant contact with the rail tracks, the lateral vibrations of the car body, including lateral and yaw motions, are the primary factors that determine ride comfort and quality. Rail vehicles have conical wheels which experience large horizontal forces called creep forces at the rail-wheel interface. These horizontal forces are responsible for steering and centering the rail vehicle, but also have undesirable effects, such as wear and energy loss [5]. Lateral instabilities can cause severe unwanted self-oscillations in rail vehicles. This phenomenon is commonly known as hunting.

Table 3.1: Model Degrees of Freedom (DOF)

Passenger Car Lateral Response Model Degrees of Freedom			
Component	**Lateral**	**Roll**	**Yaw**
Car Body	y_c	θ_c	ψ_c
Front Truck frame	y_{t1}	θ_{t1}	ψ_{t1}
Rear Truck Frame	y_{t2}	θ_{t2}	ψ_{t2}
Front Wheelset (leading)	y_{w1}	–	ψ_{w1}
Front Wheelset (trailing)	y_{w2}	–	ψ_{w2}
Rear Wheelset (leading)	y_{w3}	–	ψ_{w3}
Rear Wheelset (trailing)	y_{w4}	–	ψ_{w4}

3.1 Equations of Motion

This thesis derives and implements a linearized model of a rigid rail vehicle, with passive and active suspension elements, on a tangent track for lateral stability [5, 6, 17, 18, 37]. The full vehicle is modeled as a four-axle passenger car with two bogies. The control forces represented by $Q_{(\cdot)}$ are defined in later sections. All geometric parameters are depicted in Fig. 3.1, and are detailed in the Nomenclature section. Review of the existing literature (c.f. Chapter 1) led to the selection of the two following models with different complexities:

- Simplified Linearized 7-DOF Model for Lateral Stability of a Bogie
- Complete Linearized 17-DOF Model for Lateral Stability of a Passenger Railcar

The 17-DOF model includes the lateral and yaw DOF for each component present in the typical passenger rail car, illustrated in Fig. 3.1. The 7-DOF model is a simplified model that includes only the DOF associated with a bogie and two wheelsets. Roll DOF of the wheelsets are not included since the rail vehicle is assumed to maintain contact with the rail track at all times.

3.2 Rail Vehicle Dynamics

The governing equations of motion for the lateral displacement, y_c, yaw displacement, ψ_c and roll displacement, θ_c, are given by the following equations:

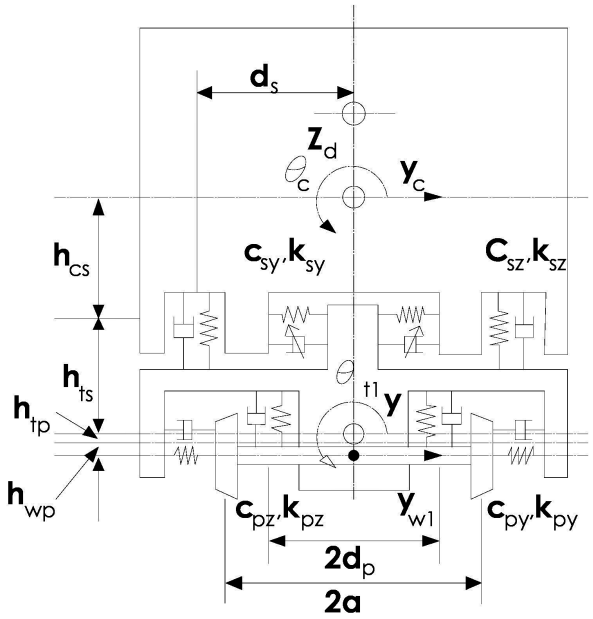

(a)

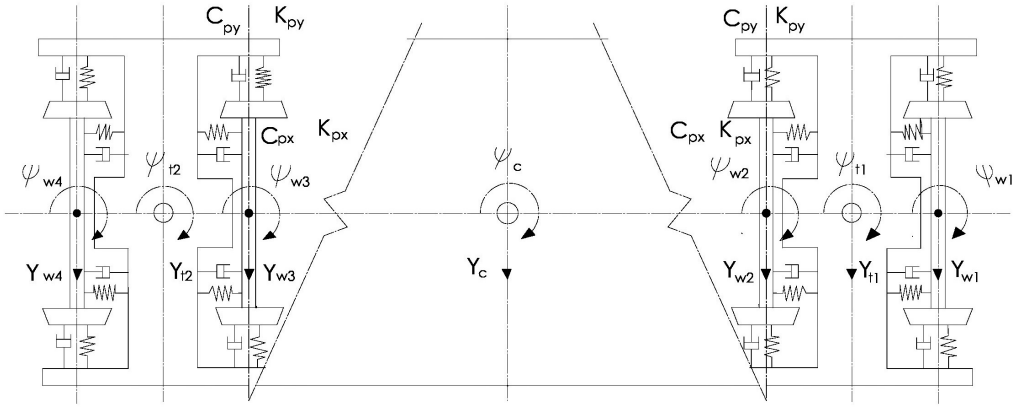

(b)

Figure 3.1: Representation of rail vehicle suspension elements and geometric parameters. Side (a) and top (b) views.

Car Body Lateral

$$m_c\ddot{y}_c + (F_{sylr} + F_{syll} + F_{sytr} + F_{sytl}) \;=\; Q_{yc} \tag{3.1}$$

where:

$$\begin{aligned} F_{syl} &= 2k_{sy}(y_c + l\psi_c + h_{cs}\theta_c - y_{t1} + h_{ts}\theta_{t1}) \\ &\quad + 2c_{sy}(\dot{y}_c + l\dot{\psi}_c + h_{cs}\dot{\theta}_c - \dot{y}_{t1} + h_{ts}\dot{\theta}_{t1}) \qquad (3.1a) \\ F_{syt} &= 2k_{sy}(y_c - l\psi_c + h_{cs}\theta_c - y_{t2} + h_{ts}\theta_{t2}) \\ &\quad + 2c_{sy}(\dot{y}_c - l\dot{\psi}_c + h_{cs}\dot{\theta}_c - \dot{y}_{t2} + h_{ts}\dot{\theta}_{t2}) \qquad (3.1b) \\ F_{syll} &= F_{sylr} = \tfrac{1}{2}F_{syl}\,, \quad F_{sytl} = F_{sytr} = \tfrac{1}{2}F_{syt} \end{aligned}$$

Car Body Yaw

$$\begin{aligned} &I_{cz}\ddot{\psi}_c - (F_{sxlr} + F_{sxtr})d_s + (F_{sxll} + F_{sxtl})d_s \\ &\quad + (F_{sylr} + F_{syll})l - (F_{sytr} + F_{sytl})l \;=\; Q_{\psi c} \end{aligned} \tag{3.2}$$

where:

$$\begin{aligned} F_{sxlr} &= -k_{sx}(\psi_c - \psi_{t1})d_s - c_{sx}(\dot{\psi}_c - \dot{\psi}_{t1})d_s \qquad (3.2a) \\ F_{sxtr} &= -k_{sx}(\psi_c - \psi_{t2})d_s - c_{sx}(\dot{\psi}_c - \dot{\psi}_{t2})d_s \qquad (3.2b) \\ F_{sxll} &= -F_{sxlr}\,, \quad F_{sxtl} = -F_{sxtr} \end{aligned}$$

Car Body Roll

$$\begin{aligned} &I_{cx}\ddot{\theta}_c - (F_{sylr} + F_{syll} + F_{sytr} + F_{sytl})h_{cs} \\ &\quad - (F_{szlr} + F_{sztr})d_s + (F_{szll} + F_{sztl})d_s \;=\; Q_{\theta c} \end{aligned} \tag{3.3}$$

where:

$$\begin{aligned} F_{szlr} &= -k_{sz}d_s(\theta_c - \theta_{t1}) - c_{sz}d_s(\dot{\theta}_c - \dot{\theta}_{t1}) \qquad (3.3a) \\ F_{sztr} &= -k_{sz}d_s(\theta_c - \theta_{t2}) - c_{sz}d_s(\dot{\theta}_c - \dot{\theta}_{t2}) \qquad (3.3b) \\ F_{szll} &= -F_{szlr}\,, \quad F_{sztl} = -F_{sztr} \end{aligned}$$

There are two trucks in the rail vehicle, the leading (l) truck and trailing (t) truck, each of which is connected to two wheelsets. The truck dynamics

for lateral stability are also characterized by the same degrees of freedom as the car body, namely, truck lateral displacement, y_{ti}, truck yaw displacement, ψ_{ti}, and truck roll displacement, θ_{ti}, where the subscript $i \in \{1, 2\}$ indicates leading or trailing truck, respectively. For $i = 1,\ m = 1, n = 2$; for $i = 2,\ m = 3, n = 4$, thus representing each wheelset of the system.

Truck Lateral

$$m_t\ddot{y}_{ti} - (F_{sylr} + F_{syll}) + (F_{pymr} + F_{pynr} + F_{pyml} + F_{pynl}) \ = \ Q_{yti} \qquad (3.4)$$

where:

$$\begin{aligned} F_{pym} &= 2k_{py}(y_{t1} - h_{tp}\theta_{t1} + b\psi_{t1} - y_{w1}) \\ &\quad + 2c_{py}(\dot{y}_{t1} - h_{tp}\dot{\theta}_{t1} + b\dot{\psi}_{t1} - \dot{y}_{w1}) \qquad (3.4a) \\ F_{pyn} &= 2k_{py}(y_{t1} - h_{tp}\theta_{t1} + b\psi_{t1} - y_{w2}) \\ &\quad + 2c_{py}(\dot{y}_{t1} - h_{tp}\dot{\theta}_{t1} + b\dot{\psi}_{t1} - \dot{y}_{w2}) \qquad (3.4b) \\ F_{pyml} &= F_{pymr} = \tfrac{1}{2}F_{pym}\ , \quad F_{pynl} = F_{pynr} = \tfrac{1}{2}F_{pyn} \end{aligned}$$

Truck Yaw

$$\begin{aligned} &I_{tz}\ddot{\psi}_{ti} - (-F_{sxlr} + F_{sxll})d_s + (F_{pxmr} + F_{pxnr})d_p \\ &\quad - (F_{pxml} + F_{pxnl})d_p + (F_{pymr} + F_{pyml})b - (F_{pynr} + F_{pynl})b \ = \ Q_{\psi_{ti}} \qquad (3.5) \end{aligned}$$

where:

$$\begin{aligned} F_{pxmr} &= k_{px}(\psi_{ti} - \psi_{wm})d_p + c_{px}(\dot{\psi}_{ti} - \dot{\psi}_{wm})d_p \qquad (3.5a) \\ F_{pxnr} &= k_{px}(\psi_{ti} - \psi_{wn})d_p + c_{px}(\dot{\psi}_{ti} - \dot{\psi}_{wn})d_p \qquad (3.5b) \\ F_{pxml} &= -F_{pxmr}\ , \quad F_{pxnl} = -F_{pxnr} \end{aligned}$$

Truck Roll

$$\begin{aligned} &I_{tx}\ddot{\theta}_{ti} - (F_{sylr} + F_{syll})h_{ts} - (F_{szlr} - F_{szll})d_s \\ &\quad - (F_{pymr} + F_{pynr} + F_{pyml} + F_{pynl})h_{tp} \\ &\quad - (F_{pzmr} + F_{pznr})d_p + (F_{pzml} + F_{pznl})d_p \ = \ Q_{\theta_{ti}} \qquad (3.6) \end{aligned}$$

where:

$$F_{pzmr} = -k_{pz} d_p \theta_{ti} - c_{pz} d_p \dot{\theta}_{ti} \tag{3.6a}$$

$$F_{pznr} = -k_{pz} d_p \theta_{ti} - c_{pz} d_p \dot{\theta}_{ti} \tag{3.6b}$$

$$F_{pzml} = -F_{pxmr}\,, \quad F_{pznl} = -F_{pznr}$$

The forces due to the rail-wheel contact are modeled based on Kalker's linear creep model [38] for rolling contact of two elastic bodies in the presence of dry friction. The lateral displacement y_{wk} and yaw displacement ψ_{wk}, where the subscript $k \in \{1, 2\}$ for the leading bogie and $k \in \{3, 4\}$ for the trailing bogie:

Wheelset Lateral

$$\begin{aligned} m_w \ddot{y}_{wk} - (F_{pykr} + F_{pykl}) + \left(+2f_{11} \left[\frac{1}{V} \left(1 + \frac{\sigma r_0}{a} \right) \dot{y}_{wk} - \psi_{wk} \right] \right) + K_{gy} y_{wk} \\ = -(2f_{11} \left[-\frac{\sigma r_0}{Va} \dot{y}_{ak} - \frac{\sigma {r_0}^2}{Va} \dot{\theta}_{clk} \right] - K_{gy}(-y_{ak} - r_0 \theta_{clk}) + Q_{y_{wk}} \end{aligned} \tag{3.7}$$

Wheelset Yaw

$$\begin{aligned} I_{wz} \ddot{\psi}_{wk} - (-F_{pxkr} + F_{pxkl}) d_p + 2f_{33} \left[\frac{\lambda_e a}{r_0} y_{wk} + \frac{a^2}{V} \dot{\psi}_{wk} \right] - K_{g\psi} \psi_{wk} \\ = -2f_{33} \left[\frac{\lambda_e a}{r_0} (-y_{ak} - r_0 \theta_{clk}) \right] + Q_{\psi_{wk}} \end{aligned} \tag{3.8}$$

3.3 Track Disturbances

The track disturbances are the primary dynamic inputs to the rail vehicles, occurring at the rail-wheel contacts. Irregularities in tracks may occur due to weld joints, misalignment, uneven rail heights, fatigue due to track loading, and many other factors. Analytically, track disturbances are represented as vertical, cross-level alignment and gauge irregularities.

This thesis makes use of the lateral alignment and cross-level irregularities relevant to the lateral stability of rail vehicles [17]. They can be defined as:

Lateral Alignment

$$y_a = \frac{y_l + y_r}{2} \tag{3.9}$$

Cross-level

$$z_{cl} = z_l + z_r \tag{3.10}$$

$$\theta_{cl} = \frac{z_{cl}}{2a} \tag{3.11}$$

where y_r and y_l represent the lateral track irregularities of the left and right rails respectively, z_r and z_l represent the vertical track irregularities of the left and right rails, respectively, and a is half of the wheelset contact distance. Here gauge deficiency is not considered, thus the lateral positions of the left and right wheels on the rails are identical.

The disturbances are modeled as periodical irregularities:

$$\theta_{cl} = \frac{1}{a} \sum_n A_n \cos n\Omega x \,, \quad n = 1, 3, 5, ... \tag{3.12}$$

Similarly:

$$y_a = \frac{4A_a}{\pi} \left[\frac{1}{3} \cos \Omega x - \frac{1}{15} \cos 2\Omega x + \frac{1}{35} \cos 3\Omega x - ... \right] \tag{3.13}$$

where A_a and A_n are scalar factors of the periodical alignment irregularities of the track with values in the range $0.59233 \times 10^{-6} \leq A \leq 1.568 \times 10^{-6}$. Ω is the spatial frequency in rad/m, which may be calculated using:

$$\omega = V\Omega, \quad \Omega = \frac{2\pi}{L} \tag{3.14}$$

where V is the velocity of the rail vehicle, ω is the angular frequency, and L is the spatial wave length of rails.

The front wheelset will experience a disturbance excitation first, followed by the trailing wheelsets. This delay time for each wheelset is defined as:

$$t_{w1} = 0 \,, \quad t_{w2} = \frac{V}{2b} \,, \quad t_{w3} = \frac{V}{2l} \,, \quad t_{w4} = \frac{V}{2(b+l)} \tag{3.15}$$

We can now define the displacement component, w, and the velocity com-

ponent, $\dot{w}$, of the disturbances,

$$w = \begin{bmatrix} y_a \\ \theta_{cl} \end{bmatrix}, \qquad \dot{w} = \begin{bmatrix} \dot{y}_a \\ \dot{\theta}_{cl} \end{bmatrix} \tag{3.16}$$

3.4 MR Damper

Magneto-rheological (MR) dampers typically consist of micron-sized, magnetically polarizable particles dispersed in a carrier medium such as mineral or silicone oil. When a magnetic field is applied to the fluids, particle chains form and the fluid becomes a semisolid and exhibits visco-plastic behavior, similar to that of ER fluids. Transition to rheological equilibrium can be achieved in a few milliseconds, allowing construction of devices with high bandwidth [4]. This magnetic field is controlled by passing current or changing the potential difference across coils that surround the damper fluid. MR dampers can operate through a wide range of temperatures and stress loading conditions. Modeling MR dampers is challenging due to its strong hysteric characteristics.

This thesis utilizes a phenomenological model based on the Bouc-Wen hysteretic model developed by Spencer [4] that has been used extensively by other researchers for the purpose of rail vehicle suspensions [17, 19, 39, 40]. Figure 3.2 represents the mechanical model of a typical Bouc-Wen MR Damper. The following mathematical model is used to simulate the characteristics of an MR Damper:

$$f = c_1\dot{y} + k_1 x - x_0 \tag{3.17}$$

where f is the damping force, x is the displacement of the MR Damper, x_0 is the initial displacement, k_1 is the stiffness of the internal accumulator associated with the nominal damping force, and y is the internal displacement of the damper. Further, the displacement dynamics can be modeled as:

$$\dot{y} = \frac{1}{c_0 + c_1}[\alpha z + c_0\dot{x} + k_0(x - y)] \tag{3.18}$$

$$\dot{z} = -\gamma|\dot{x} - \dot{y}||z|^{n-1}z - \beta(\dot{x} - \dot{y})|z|^n + A_{mr}(\dot{x} - \dot{y}) \tag{3.19}$$

where z is an evolutionary variable that determines hysteresis behavior in

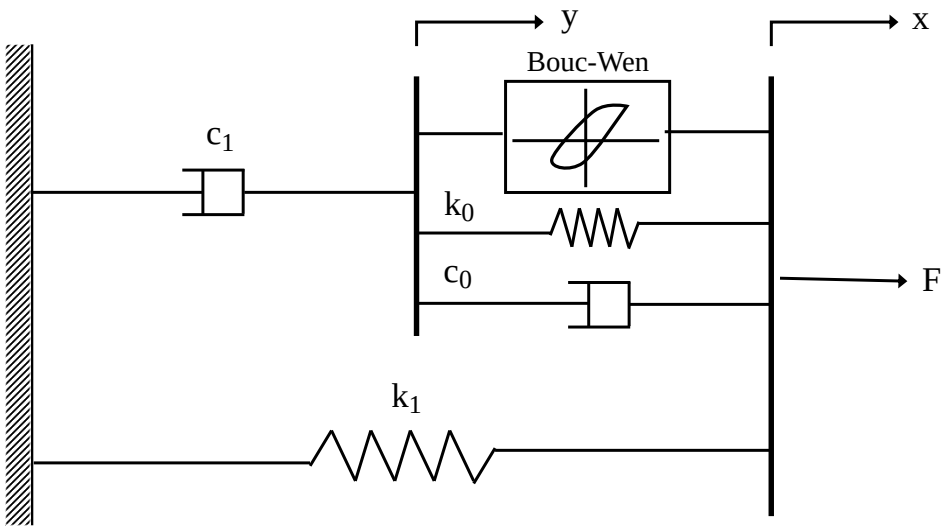

Figure 3.2: Mechanical model for the magneto-rheologoical (MR) damper [4]

conjunction with other shape parameters, including c_0, c_1, α, γ, β, and A_{mr}. The coefficients of certain parameters in Prob. (3.18) can be given by the following equations:

$$\alpha = \alpha(u) = \alpha_a + \alpha_b u \tag{3.20}$$

$$c_1 = c_1(u) = c_{1a} + c_{1b} u \tag{3.21}$$

$$c_0 = c_0(u) = c_{0a} + c_{0b} u \tag{3.22}$$

where u is the output of a first order filter given by:

$$\dot{u} = -\eta(u - v) \tag{3.23}$$

and v is the command voltage to the current driver of the damper.

3.5 System Modeling

Lateral vibrations are the most significant contributors to the undesirable hunting phenomenon. Hunting arises from the interaction of adhesion forces and inertial forces. At low speeds, adhesion dominates but, as the speed increases, the adhesion forces and inertial forces become comparable in mag-

nitude. Oscillation may occur above a critical vehicle speed. Above this speed, the motion can be violent, damaging the track and wheels, and potentially causing derailment [41]. In this thesis, active control is added to the lateral suspension system to achieve maximum ride comfort, increase ride quality, and mitigate hunting at higher speeds.

Three different active control phenomena are tested:

- Active control using damping force
- Semi-active control, modeled using a damping coefficient for linear damper
- Semi-active control, modeled using the MR damper model described above

These control techniques are tested for two models of increasing complexity based on the equations of motion derived in Section 3.1.

3.5.1 7-DOF Model

The first model is a 7-DOF linear model that is comprised of two wheelsets connected to one bogie through the primary suspension. The secondary suspension is omitted in this model. This model provides a baseline for a more complex full rail car analysis which will be analyzed subsequently. Four controlled dampers with forces, f_{pylr}, f_{pyll}, f_{pytr}, and f_{pytl}, are added to the primary lateral damping. The passive dampers are removed for the active control analysis. Equations (3.4) – (3.8) are used to model this system with $i = 1$, $m = 1$, $n = 2$, $k = 1, 2$, where the control forces, $Q_{(\cdot)}$, can be defined as:

$$Q_{y_{t1}} = f_{pylr} + f_{pyll} + f_{pytr} + f_{pytl} \tag{3.24a}$$

$$Q_{\psi_{t1}} = (f_{pylr} + f_{pyll})b - (f_{pytr} + f_{pytl})b \tag{3.24b}$$

$$Q_{\theta_{t1}} = -(f_{pylr} + f_{pyll} + f_{pytr} + f_{pytl})h_{tp} \tag{3.24c}$$

$$Q_{y_{w1}} = -f_{pylr} - f_{pyll} \tag{3.24d}$$

$$Q_{\psi_{w1}} = 0 \tag{3.24e}$$

$$Q_{y_{w2}} = -f_{pytr} - f_{pytl} \tag{3.24f}$$

$$Q_{\psi_{w2}} = 0 \tag{3.24g}$$

The equations of motion can now be rewritten as:

$$\mathbf{M}\ddot{\mathbf{y}} + \mathbf{C}\dot{\mathbf{y}} + \mathbf{K}\mathbf{y} = \mathbf{F_u}\mathbf{u} + \mathbf{F_w}\mathbf{w} + \mathbf{F_{\dot{w}}}\dot{\mathbf{w}} \tag{3.25}$$

where $\mathbf{M}(\in \mathbb{R}^{7\times7})$ is the mass matrix, $\mathbf{C}(\in \mathbb{R}^{7\times7})$ is the damping matrix, $\mathbf{K}(\in \mathbb{R}^{7\times7})$ is the stiffness matrix, $\mathbf{F_u}(\in \mathbb{R}^{7\times4})$ is the control force coefficient matrix, $\mathbf{F_w}, \mathbf{F_{\dot{w}}}(\in \mathbb{R}^{7\times2})$ are the track irregularities coefficient matrices, and:

$$\begin{gathered} y = \begin{bmatrix} y_{t1} & \psi_{t1} & \theta_{t1} & y_{w1} & \psi_{w1} & y_{w2} & \psi_{w2} \end{bmatrix}, \\ u = \begin{bmatrix} f_{pylr} & f_{pyll} & f_{pytr} & f_{pytl} \end{bmatrix}, \\ w = \begin{bmatrix} y_{a1} & y_{a2} & \theta_{cl1} & \theta_{cl2} \end{bmatrix}, \quad \dot{w} = \begin{bmatrix} \dot{y}_{a1} & \dot{y}_{a2} & \dot{\theta}_{cl1} & \dot{\theta}_{cl2} \end{bmatrix} \end{gathered} \tag{3.26}$$

This allows us to define a state vector, $\boldsymbol{\xi} = [\mathbf{y}\ \dot{\mathbf{y}}]^\intercal$, and using the equations of motion, a state-space model can be formulated as:

$$\dot{\boldsymbol{\xi}} = \mathbf{A}\boldsymbol{\xi} + \mathbf{B}\mathbf{u} + \mathbf{E_w}\mathbf{w} + \mathbf{E_{\dot{w}}}\dot{\mathbf{w}} \tag{3.27}$$

where,

$$\begin{gathered} \mathbf{A} = \begin{bmatrix} 0_{7\times7} & I_{7\times7} \\ M^{-1}K & M^{-1}C \end{bmatrix}, \mathbf{B} = \begin{bmatrix} 0_{7\times7} \\ M^{-1}F_u \end{bmatrix}, \\ \mathbf{E_w} = \begin{bmatrix} 0_{7\times7} \\ M^{-1}F_w \end{bmatrix}, \mathbf{E_{\dot{w}}} = \begin{bmatrix} 0_{7\times7} \\ M^{-1}F_{\dot{w}} \end{bmatrix} \end{gathered} \tag{3.28}$$

3.5.2 17-DOF Model

A full-scale, linearized model of a rigid rail vehicle is developed with 17-DOF, using Eqns. (3.1)–(3.8), identically. The model contains one passenger car body attached to two bogies, each of which is attached to two wheelsets as illustrated in Fig. 3.1. Four controlled dampers with forces, f_{sylr}, f_{syll}, f_{sytr}, and f_{sytl}, are added to the secondary lateral damping, and the passive dampers are removed for the active control analysis. Track level alignment and cross level as described in Eqns. (3.7), (3.8), and (3.16) are regarded as external excitations to the vehicle, given to each wheelset with time delays

defined in Eqn. (3.15). The control force equations, $Q_{(\cdot)}$, for the full-scale model can now be defined as:

$$Q_{y_c} = f_{sylr} + f_{syll} + f_{sytr} + f_{sytl} \tag{3.29a}$$
$$Q_{\psi_c} = (f_{sylr} + f_{syll})l_s - (f_{sytr} + f_{sytl})l_s \tag{3.29b}$$
$$Q_{\theta_c} = -(f_{sylr} + f_{syll} + f_{sytr} + f_{sytl})h_{cs} \tag{3.29c}$$
$$Q_{y_{t1}} = -f_{sylr} - f_{syll} \tag{3.29d}$$
$$Q_{\psi_{t1}} = 0 \tag{3.29e}$$
$$Q_{\theta_{t1}} = -(f_{sylr} + f_{syll})h_{ts} \tag{3.29f}$$
$$Q_{y_{t2}} = -f_{sytr} - f_{sytl} \tag{3.29g}$$
$$Q_{\psi_{t2}} = 0 \tag{3.29h}$$
$$Q_{\theta_{t2}} = -(f_{sytr} + f_{sytl})h_{ts} \tag{3.29i}$$
$$Q_{y_{wk}} = 0 \tag{3.29j}$$
$$Q_{\psi_{wk}} = 0 \tag{3.29k}$$

The equations of motion can now be rearranged and formulated as a state-space model, similar to Eqn. (3.25). For the sake of brevity, individual component vectors, as described in Eqn. (3.26), are omitted in this section. The final state space matrices can be constructed as:

$$\mathbf{A} = \begin{bmatrix} 0_{17\times17} & I_{17\times17} \\ M^{-1}K & M^{-1}C \end{bmatrix}, \mathbf{B} = \begin{bmatrix} 0_{17\times17} \\ M^{-1}F_u \end{bmatrix},$$

$$\mathbf{E_w} = \begin{bmatrix} 0_{17\times17} \\ M^{-1}F_w \end{bmatrix}, \mathbf{E_{\dot{w}}} = \begin{bmatrix} 0_{17\times17} \\ M^{-1}F_{\dot{w}} \end{bmatrix} \tag{3.30}$$

where $\mathbf{M}(\in \mathbb{R}^{17\times17})$ is the mass matrix, $\mathbf{C}(\in \mathbb{R}^{17\times17})$ is the damping matrix, $\mathbf{K}(\in \mathbb{R}^{17\times17})$ is the stiffness matrix, $\mathbf{F_u}(\in \mathbb{R}^{17\times4})$ is the control force coefficient matrix, and $\mathbf{F_w}, \mathbf{F_{\dot{w}}}(\in \mathbb{R}^{17\times4})$ are the track irregularities coefficient matrices.

Chapter 4

Numerical Studies

The simultaneous co-design formulation discussed in Chapter 2 is applied to optimizing the performance of rail vehicles based on models presented in Chapter 3. For each model, 7-DOF and 17-DOF, three different control techniques—active control using force, semi-active control using damping coefficient, and semi-active control using MR dampers—are designed using the simultaneous DT approach 2.10. The comfort of a passenger in a rail car is dependent on the magnitude and frequencies of accelerations felt. Appropriate performance indices (objective functions), encapsulating the effects of these accelerations felt over time traveled, are formulated.

The active control problem is solved first to obtain the actuator force trajectory (time history) that minimizes the selected performance index. No assumptions are made on actuator structure, and liberal force bounds are used. This solution serves as a benchmark for maximum system performance and other semi-active applications. The open-loop active force may be realized using electric or pneumatic actuators, but such actuators usually require prohibitively high power, hindering practical implementation [3].

The solution for the active control case is followed by a solution for optimal damping trajectory using a linear damper. The damping coefficient for a linear damping model is used as the control input. Based on velocity (state), this coefficient determines the damping force. This idealized semi-active control problem accounts for some realistic restrictions on realizable adaptive dampers, and the results aid in determining appropriate selection of MR dampers for the vehicle. Properties of MR dampers were discussed in Chapter 1.

Following the design of the control problems above, a decision can be made regarding the voltage bounds required for the MR damper. At this step, a semi-active control problem using the previously-modeled MR damper (see Section 3.4) is solved using a simultaneous co-design approach. This problem

was modeled as an NLP due to the inherent non-linearities of an MR damper. Plant design variables are chosen appropriately for each problem, and are included as optimization variables in the co-design formulation. The reason for choosing simultaneous co-design will be discussed in the later sections.

4.1 MR Damper

Before solving the optimization problem, we simulate the characteristics of the MR damper modeled in Section 3.4, for different control voltages. Force is modeled as function of time, displacement and velocity in Figs. 4.1(a)-(c) to observe the hysteric shape characteristics. A displacement of amplitude of 6.35 mm and frequency of 10 Hz is used for the simulations.

Although the MR damper model is effective for any desired frequency and amplitude combination, Fig. 4.1 shows the stability of the damper for the selected value of parameters. For the chosen values of input voltage, the force limits indicate that the selected damper model should be able to generate the control force required to attenuate unwanted vehicle vibrations. Simulations of the system using only passive elements (based on reference parameter values [16]) were used to support the determination of these bounds for the input voltage of the MR Damper.

4.2 Co-Design of a Reduced 7-DOF Model

The reduced model as described in Section 3.5.1 represents a typical rail truck (bogie). The performance index, to use with the simultaneous co-design approach defined in Prob. (2.9), is the minimization of the combined effect of lateral, $\ddot{y}$, yaw, $\ddot{\psi}$, and roll, $\ddot{\theta}$, accelerations of the rail truck over time. The simultaneous co-design formulation, assuming fully-active control, is:

$$\min_{\mathbf{x_c},\mathbf{x_p}} \quad \psi = \int_{t_0}^{t_f} \left[\rho_1 \ddot{y}_{t1}^2 + \rho_2 \ddot{\psi}_{t1}^2 + \rho_3 \ddot{\theta}_{t1}^2\right] dt \tag{4.1a}$$

$$\text{s.t.} \quad \dot{\boldsymbol{\xi}}(t) - \mathbf{f}(\boldsymbol{\xi}(t), \mathbf{x_c}, \mathbf{x_p}, t) = \mathbf{0}. \tag{4.1b}$$

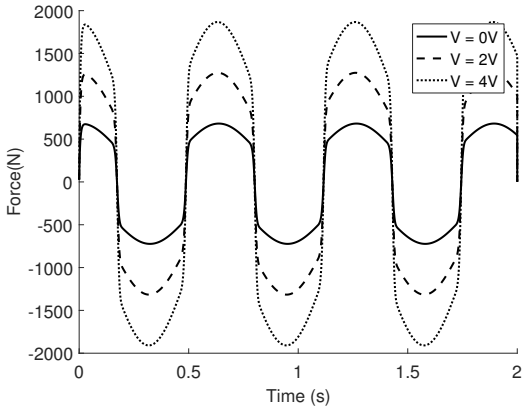

(a)

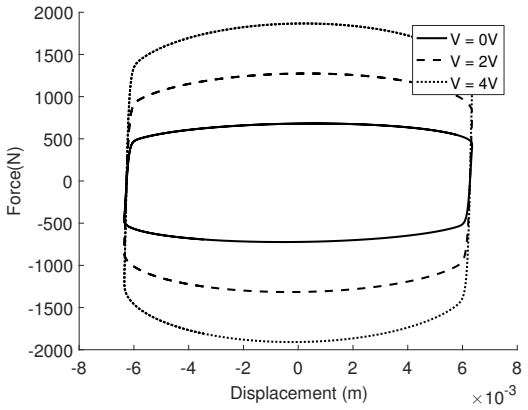

(b)

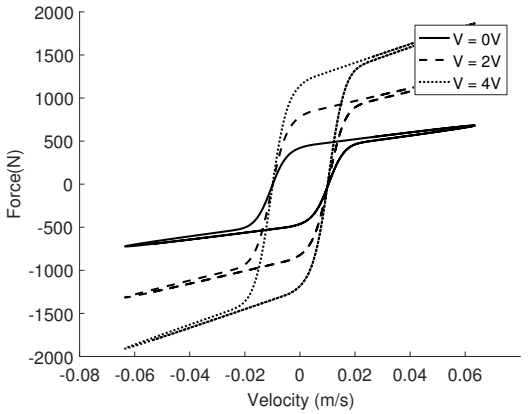

(c)

Figure 4.1: Simulating a magneto-rheological damper: (a) Hysteresis Force vs. Time (b) Hysteresis Force vs. Displacement (c) Hysteresis Force vs. Velocity

Table 4.1: Comparing different control techniques for the lateral stability of a 7-DOF system

Control Technique	Objective Function	Plant Design Variable	
		k_{px} (N/m)	k_{py} (N/m)
P1 : Force	0.0256	9.8199×10^7	1.001×10^5
P2 : Damping - Linear Damper	0.2180	5.6276×10^7	9.0867×10^5
P3 : Voltage - MR Damper	5.3903	3.6081×10^6	3.5261×10^7

where $\mathbf{x_c}$ is the control force vector added to the lateral primary suspension, and $\mathbf{x_p}$ are the plant design variables, namely the primary lateral suspension stiffness, k_{py}, and longitudinal suspension stiffness, k_{px}. The dynamic constraint is defined in Prob. (3.27). The objective function weights are $\rho_1 = \rho_2 = \rho_3 = 1/3$.

The states and control are discretized through time and entered as optimization variables. The state trajectory approximation is performed using trapezoidal collocation, and solved using defect constraints. These constraints are modeled as non-linear equality constraints within the NLP formulation. No other constraints were used for the system except upper and lower bounds on control, state, and plant design variables. These bounds for state variables were based on simulations of the passive system using ordinary differential equation solvers.

Lateral, yaw and roll accelerations trajectories for each DOF obtained using simultaneous co-design of the 7-DOF system are shown and compared in Figs. 4.2 and 4.3 for different control techniques. Table 4.1 shows the objective function value and plant design variable values obtained for each strategy. **P1**, the actively controlled system, has the least design restriction and, as expected, performs the best. The next best performance is realized via solution of **P2**, followed by the performance of **P3**. Active control **P1** provides the best performance in terms of the objective function value. Semi-active control with a variable damping coefficient, **P2**, provides a marginally lower performance than **P1**, but provides significantly better performance than **P3**. **P3** is more representative of a realistic system. Better performance might be achieved with a different MR damper.

The control trajectories are plotted in Figs. 4.4–4.6. These provide an interesting insight about the use of active damping in primary suspensions. It should be noted that, while the control forces are high, the control inputs in

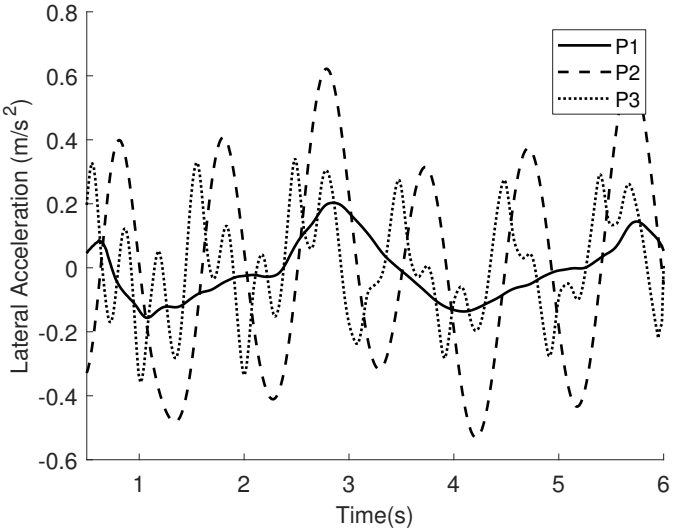

(a)

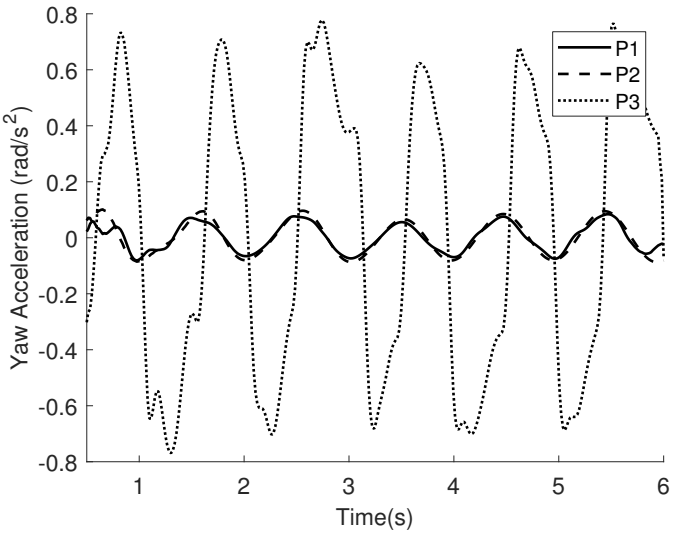

(b)

Figure 4.2: Simultaneous co-design of active control (**P1**), semi-active control using linear dampers (**P2**), and semi-active control using MR dampers (**P3**) for a 7-DOF system: Trajectories of truck (a) lateral accelerations $\ddot{y}_{t1}^2$ (b) yaw accelerations $\ddot{\psi}_{t1}^2$

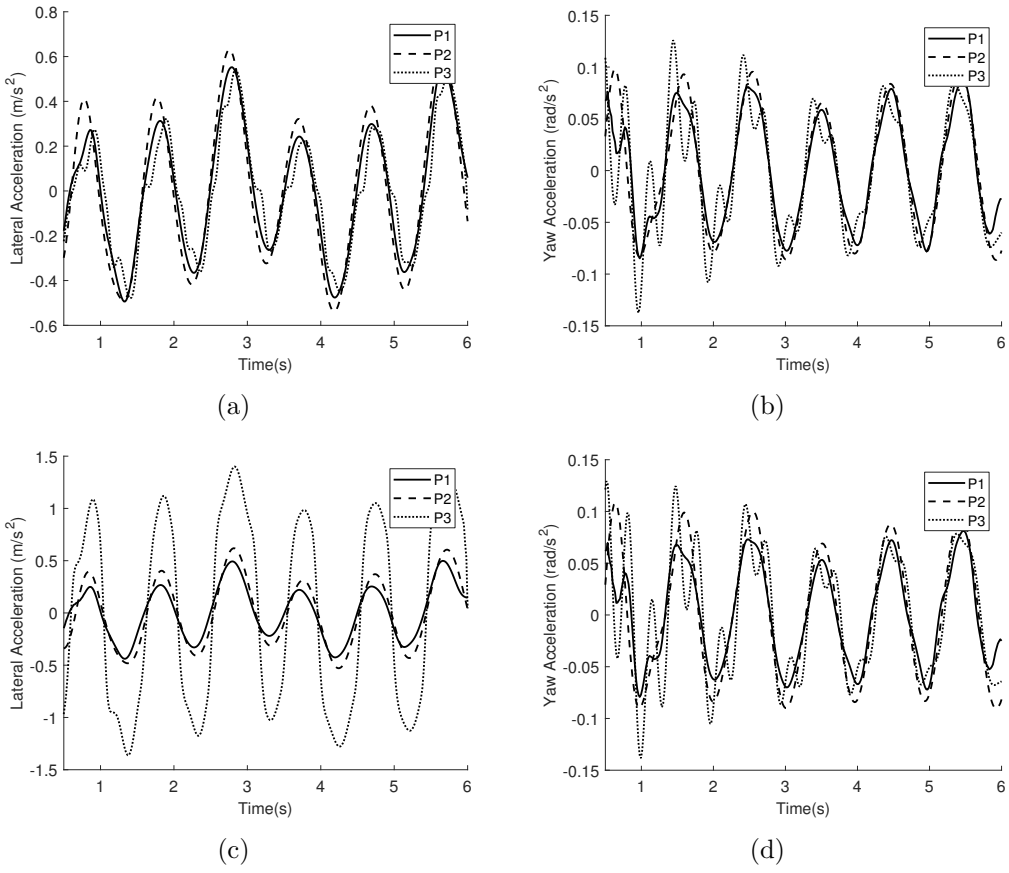

Figure 4.3: Simultaneous co-design of active control (**P1**), semi-active control using linear dampers (**P2**), and semi-active control using MR dampers (**P3**) for a 7-DOF system. Trajectories of leading wheelset: (a) lateral accelerations $\ddot{y}_{w1}^2$, and (b) yaw accelerations $\ddot{\psi}_{w1}^2$. Trajectories of trailing wheelset: (c) lateral accelerations $\ddot{y}_{w2}^2$, and (d) yaw accelerations $\ddot{\psi}_{w2}^2$.

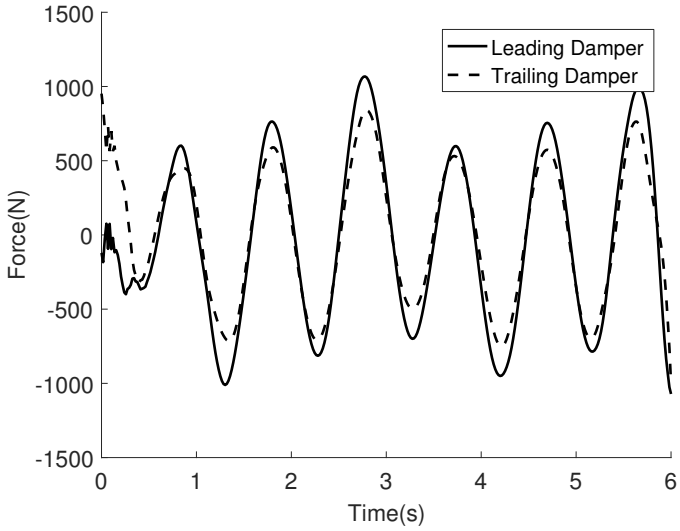

Figure 4.4: Active control (**P1**) for a 7-DOF system: Time history of damping force (N) provided by the lateral active controller

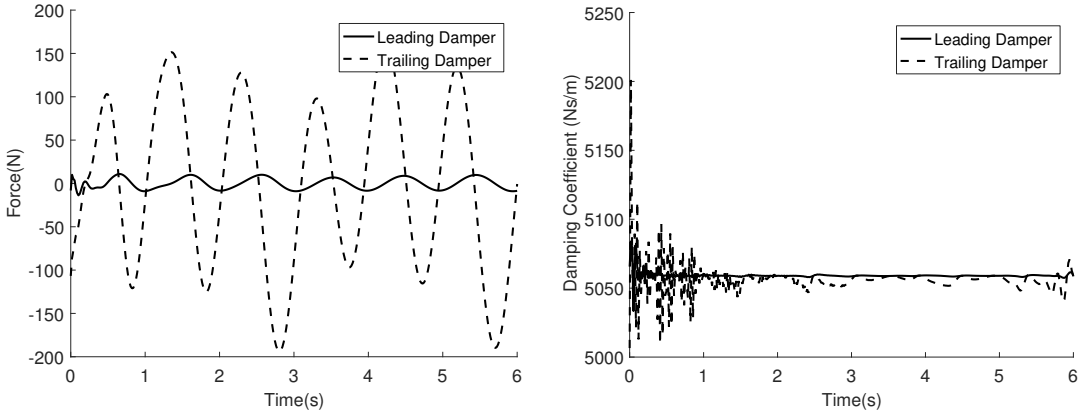

(a) (b)

Figure 4.5: Semi-active control (**P2**) for a 7-DOF system using linear dampers: Trajectories of (a) damping force (N) provided by the lateral semi-active controllers, and (b) damping coefficient (Ns/m).

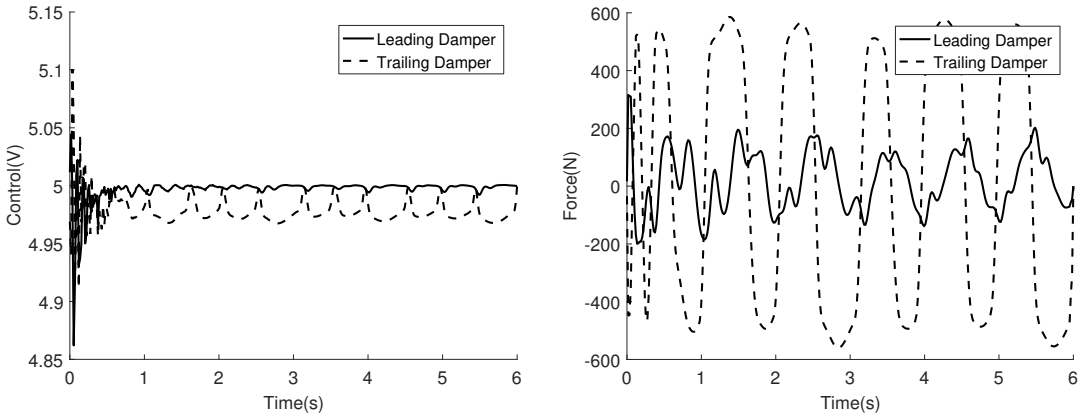

(a) (b)

Figure 4.6: Semi-active control (**P3**) for a 7-DOF system using magneto-rheological dampers: Trajectories of (a) voltage (V) applied and (b) damping force (N) provided by the lateral semi-active MR dampers

P2 and **P3** remain fairly constant. Thus, it may not be particularly useful for rail engineers to use active dampers in primary suspensions, especially because the damping requirements are very high and secondary suspension provide more room for mechatronic systems. We will see in the following sections that in the case of active secondary suspensions, control becomes more critical.

The voltage trajectory for **P3** remains constant at a value of approximately 5V, and the damping coefficient in **P2** maintains a value close to 5060 Ns/m throughout the time horizon. Hence, a passive damper with similar damping characteristics may be a satisficing solution for lateral primary damping given periodical track irregularities. Although, as the randomness in track disturbances increases this assertion may change, due to the inherent ability of active/semi-active dampers to adapt.

4.3 Co-Design of a Full Scale 17-DOF Model

The 17-DOF problem is solved for two separate plant design variable vectors: primary stiffness coefficients and secondary stiffness coefficients. A quadratic performance index [18] is used to quantify ride comfort for passengers trav-

eling in a rail vehicle:

$$\min_{\mathbf{x_c},\mathbf{x_p}} \quad \psi = \int_{t_0}^{t_f} \Big[\rho_1 y_c^2 + \rho_2 \psi_c^2 + \rho_3 \theta_c^2 + \rho_4 \sum_{i,j} f_{syij}^2 \ldots$$

$$\ldots + \rho_5 (y_{sl}^2 + y_{sl}^2) + \rho_6 \sum_{n=1}^{4} y_{ptn}^2 \Big] dt \tag{4.2a}$$

$$\text{s.t.} \quad \dot{\boldsymbol{\xi}}(t) - \mathbf{f}(\boldsymbol{\xi}(t), \mathbf{x_c}, \mathbf{x_p}, t) = \mathbf{0} \tag{4.2b}$$

where $\rho_1 = 1$, $\rho_2 = 1$, $\rho_3 = 10$, $\rho_4 = 10^{-4}$, $\rho_5 = 10^7$, $\rho_6 = 10^{-5}$, and:

$$y_{sl} = y_c + l\psi_c - \theta_c h_{cs} - (y_{t1} + \theta_{t1} h_{ts}), \tag{4.3a}$$

$$y_{st} = y_c - l\psi_c - \theta_c h_{cs} - (y_{t2} + \theta_{t2} h_{ts}), \tag{4.3b}$$

$$y_{pt1} = y_{t1} - \theta_{t1} h_{tp} + \psi_{t1} b - y_{w1}, \tag{4.3c}$$

$$y_{pt2} = y_{t1} - \theta_{t1} h_{tp} - \psi_{t1} b - y_{w2}, \tag{4.3d}$$

$$y_{pt3} = y_{t2} - \theta_{t1} h_{tp} + \psi_{t1} b - y_{w3}, \tag{4.3e}$$

$$y_{pt4} = y_{t2} - \theta_{t1} h_{tp} - \psi_{t1} b - y_{w4} \tag{4.3f}$$

For the first set of design variables, primary suspension stiffness, a simultaneous DT approach is used, similar to the 7-DOF system solution, for all three cases: active control **G1**, semi-active with linear dampers **G2**, and semi-active with MR dampers **G3**. A trend similar to the 7-DOF system is obtained. **G1** provides the best performance index with **G2** marginally behind.

Yaw and lateral acceleration trajectories of the car-body are obtained via each of these control strategies, and are plotted in Fig. 4.7. The trajectories, although delayed, appear to be identical. The control trajectories for **G2** and **G3** are displayed in Figs. 4.8 and 4.9. The control trajectories of the car body accelerations in the 17-DOF vary considerably with time due to the lateral track disturbances and irregularities. These accelerations are attenuated strongly with respect to the wheelset accelerations (Fig. 4.3) and truck accelerations (Fig. 4.2) in the 7-DOF model.

Due to the configuration of a 17-DOF model, the active secondary suspensions must withstand directional forces, at every time point, from the two rail trucks connected to four wheelsets through another suspension (the primary suspension). Compensating for these forces requires an efficient control strat-

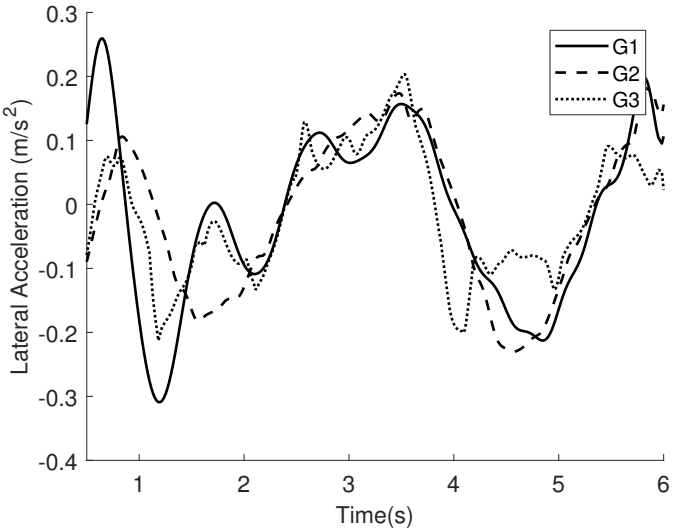

(a)

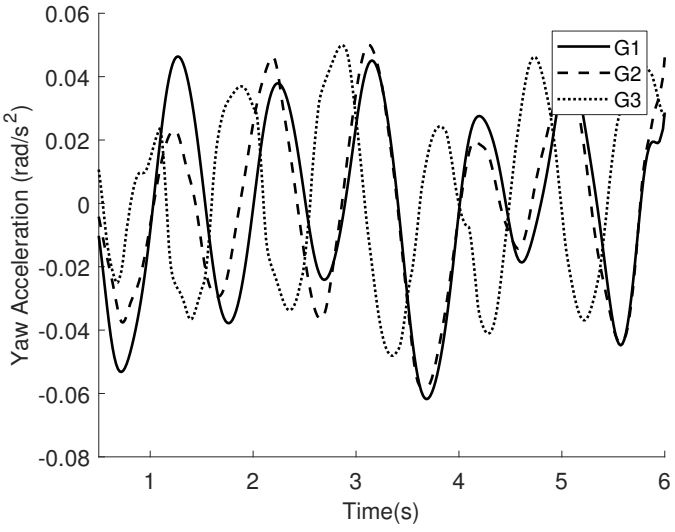

(b)

Figure 4.7: Active control (**G1**), semi-active control using linear dampers (**G2**), and semi-active control using MR dampers (**G3**) for a 17-DOF system: Trajectories of car body (a) lateral accelerations $\ddot{y}_c^2$, and (b) yaw accelerations $\ddot{\psi}_c^2$

Table 4.2: Comparing different control techniques for the lateral stability of a full-scale 17-DOF rail vehicle, with primary suspension parameters as plant design variables

Control Technique	Objective Function	Plant Design Variable	
		k_{px} (N/m)	k_{py} (N/m)
G1: Force	2.0795×10^4	9.8306×10^7	1.0000×10^5
G2: Damping - Linear Damper	2.3459×10^4	9.6332×10^7	1.0002×10^5
G3: Voltage - MR Damper	4.4957×10^4	6.3305×10^5	2.5210×10^7

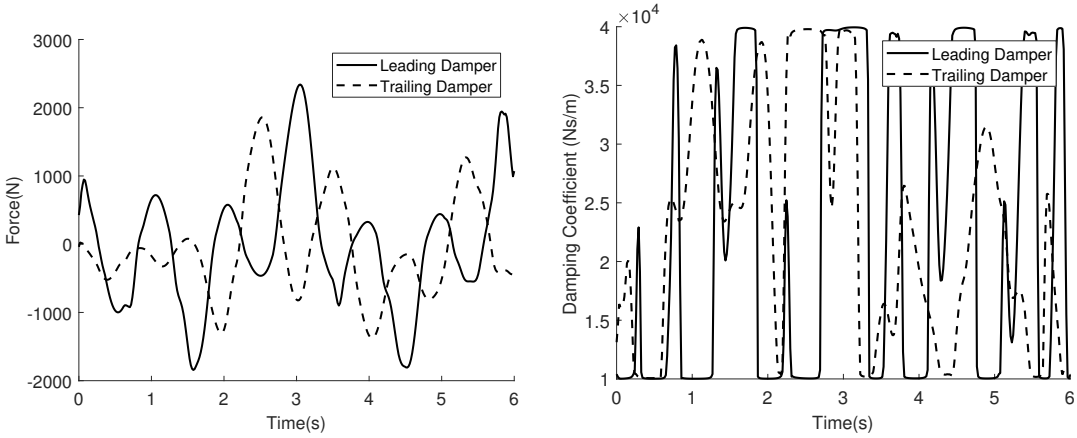

(a) (b)

Figure 4.8: Semi-active control (**G2**) for a 17-DOF system using linear dampers: Trajectories of (a) damping coefficient (Ns/m) and (b) damping force (N) provided by the lateral semi-active controllers

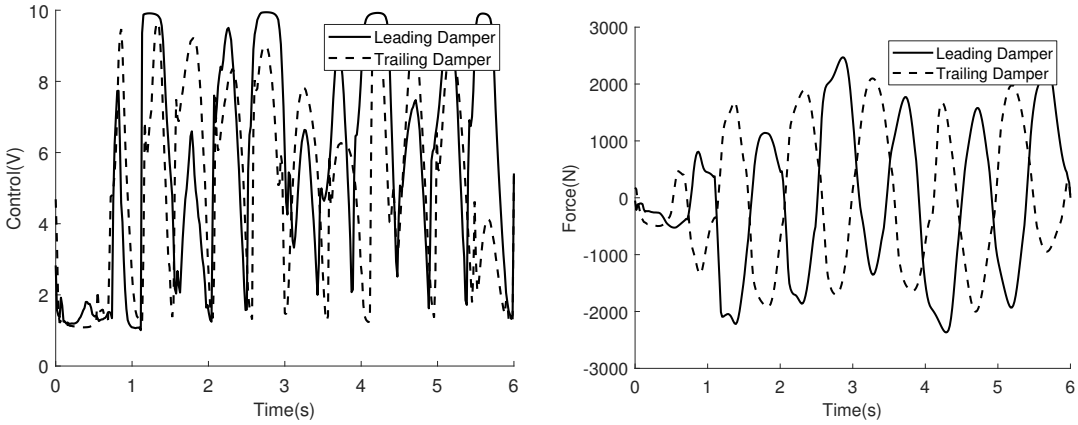

(a) (b)

Figure 4.9: Semi-active control (**G3**) for a 17-DOF system using magneto-rheological dampers: Trajectories of (a) voltage (V) applied, and (b) damping force (N) provided by the lateral semi-active MR dampers

Table 4.3: Optimal design values for each design strategy for the problem using the 17-DOF full-scale model, with secondary suspension stiffness as plant design variables

Control Technique	Objective Function	Plant Design Variable		
		k_{sx} (N/m)	k_{sy} (N/m)	k_{sz} (N/m)
S1: Simultaneous	8.89×10^2	1.68×10^6	9.90×10^7	5.19×10^6
S1: Nested (DTQP)	1.69×10^2	2.31×10^5	9.99×10^7	2.76×10^7
S2: Simultaneous	5.46×10^3	7.89×10^7	7.22×10^7	1.42×10^5
S3: Simultaneous	2.47×10^3	3.52×10^7	9.99×10^7	9.98×10^5
S4: OLC (DTQP)	3.42×10^5	3.00×10^5	1.97×10^5	6.87×10^5
S5: Passive	1.35×10^6	3.00×10^5	1.97×10^5	6.87×10^5

egy that works reliably with the controlled dampers to provide the required damping force and dissipate the required energy. While **G1** performed the best among the different techniques, it is difficult to implement fully-active suspensions due to their significantly high power demands. Hence, using semi-active dampers may prove to be fruitful for this application. Another approach that can be explored further is limiting the control authority of the fully-active system as detailed in [42]. This would help quantify the tradeoff between suspension performance and actuator size and cost. Such tradeoff curves would help determine whether the additional expense of a fully-active system (perhaps with reduced control authority) is worth the additional cost.

The final study aims to compare the proposed co-design formulations. The simultaneous DT approach used in each of the previous design solutions was chosen specifically to handle the non-linearity of magneto-rheological dampers. Non-linear programming (NLP) solver from the MATLAB [43] was used to find the local minimum for each design problem. The limitation of such NLP solvers is the inability to guarantee global optimum.

Since the selected objective function is quadratic, **S1**, the fully active control problem was solved using a linear (constraints) quadratic (objective) direct transcription based quadratic programming solver [28] (DTQP)[1]. A composite trapezoidal quadrature was used for the objective function approximation, and a trapezoidal rule collocation method was used for state estimation, similar to the nonlinear DT formulation described earlier. This

[1]The Direct Transcription Quadratic Programming (DTQP) solver has been developed by Daniel Herber, Yong-Hoon Lee, and James Allison, Engineering System Design Lab, University of Illinois Urbana-Champaign. Relevant publications and open-source code will be available in the near future.

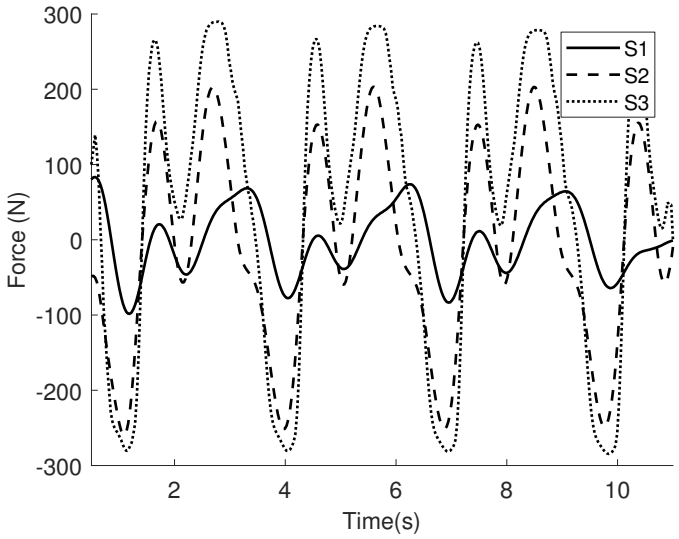

(a)

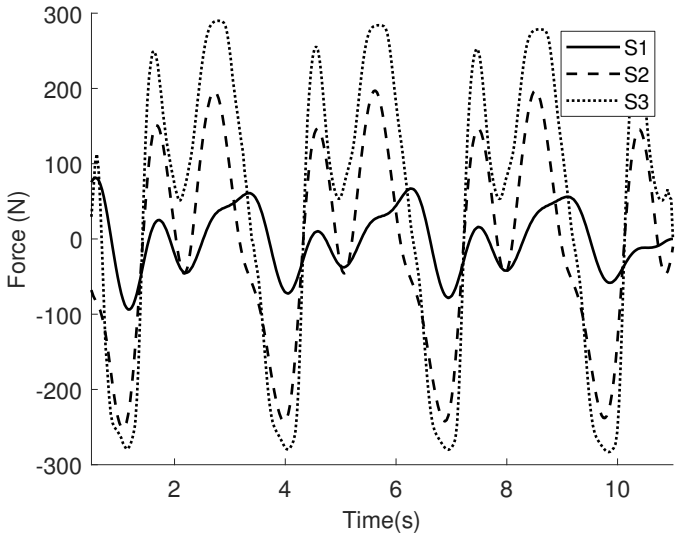

(b)

Figure 4.10: Comparison of damping forces provided by the (a) leading and (b) trailing lateral secondary suspensions using active control (**S1**), semi-active control with linear dampers (**S2**), and semi-active control with MR dampers (**S3**) for a 17-DOF system

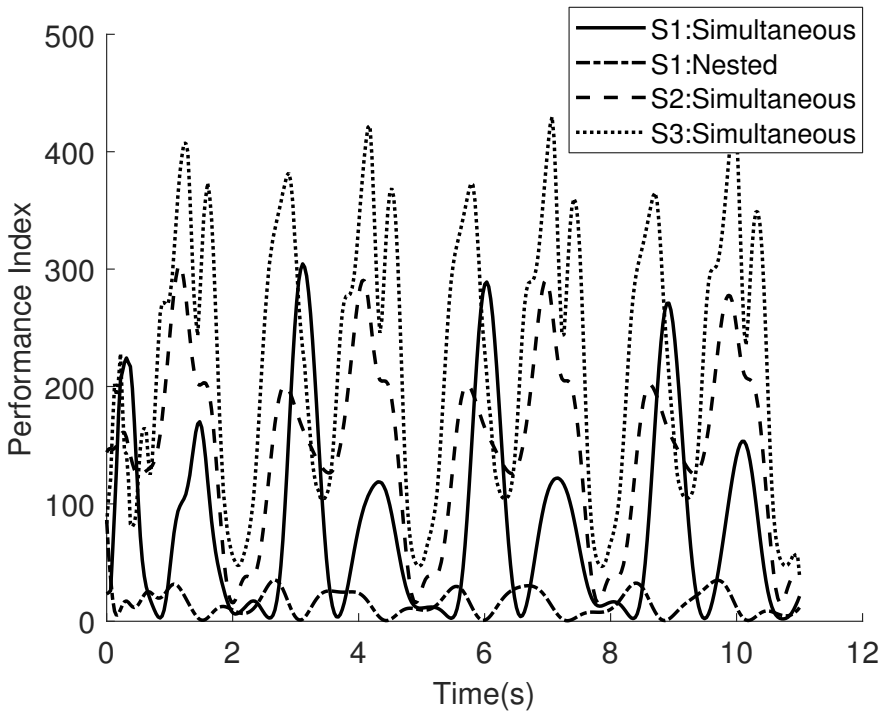

Figure 4.11: Performance index (before integration) of the different design strategies

solution method guarantees a global optimum but, cannot be used with nonlinear constraints or elements such as MR dampers. Thus, the quadratic programming (QP) solution strategy is limited to the fully-active control case.

To solve the co-design problem using the DTQP solver, a nested approach 2.3.1 was implemented. The outer loop, using a basic NLP solver, supplied plant design candidates to the inner loop problem, which was then solved for each plant design using the DTQP solver. The DTQP solver returned a globally optimal state and control variable vector for each plant design, and these trajectories were used to calculate the objective function. Results are compared in Table 4.3, including the solution of **S1** using both nested (with DTQP) and simultaneous (with nonlinear DT) co-design, as well as **S2** and **S3** using simultaneous co-design. In the final case study **S4**, we investigate the performance available when replacing the existing reference secondary lateral passive suspension elements with arbitrary force trajectories that we optimize (i.e., fully-active control elements). These results are further compared against the performance of an optimal passive system design, **S5**. The

parameters from this optimal passive system design for a 17-DOF passenger rail car model [16], were used as starting points for all parameters in each of the above mentioned solution case studies.

Table 4.3 shows that the performance of the active and semi-active suspensions is orders of magnitude improved over passive suspension systems. Adding optimal control without optimizing plant design variables, in **S4**, results in a $10\times$ improvement in the performance index. Since the performance index is based on maximizing dynamic lateral stability of the rail vehicle, such improvements in objective function value result in enhanced stability, ride quality, and comfort. Simultaneous and nested approaches of the synergistic co-design problem, result in $10^3\times$ improvements over the non-integrated approach. The results from Table 4.3 illustrate the capabilities of posing a linear (constraints) quadratic (objective) optimization problem while using co-design strategies to achieve maximum system performance. The results from simultaneous co-design can be further improved using solutions from other design methods as starting points in an NLP solver. A main result to observe here is that significant improvements are achieved over passive design and sequential design using open loop control for each co-design method.

Chapter 5

Conclusions and Future Work

In this thesis, an advanced dynamic system design approach is used to explore the limits of performance objectives for active and semi-active rail vehicle suspension systems. The thesis focused on constructing co-design formulations, modeling reduced-order and full-scale rail vehicles, and solving co-design problems for active and semi-active suspension systems. Magneto-rheological (MR) fluid dampers were investigated as a reduced-cost and power/energy alternative to fully-active suspension components. The non-linear model of MR dampers was developed based on existing phenemenological models for use with nonlinear co-design solution strategies.

Co-design exploits the synergy between plant (physical) and control design to get system-optimal solutions. Direct transcription allows us to perform simultaneous analysis and design of dynamic systems. It is used to discretize the problem over a finite time horizon. DT was used to solve a simultaneous co-design problem for several cases. The states, plant, and control variables are optimization in the simultaneous co-design problem. Local collocation methods are used to approximate states, and a quadrature method is used to approximate objective function values. The solutions obtained from co-design problems are system-optimal with respect to the models and formulations used. An alternative co-design formulation, nested, is used as well to capitalize on efficient solvers for linear-quadratic optimal control problems that can be formulated as quadratic programs using DT (as is the case with the fully-active system).

This work lays the groundwork for exploring newer design strategies for solving complex non-linear controlled dynamic systems such as rail vehicles. It motivates rail engineers to consider physical and control system design as a single cohesive problem. Integrated design methods are demonstrated to improve overall system performance by capitalizing on design coupling. Co-design methods can be applied to the design of systems with varying com-

plexities. It is observed that semi-active suspensions, specifically, those using magneto-rheological dampers, can be designed effectively using co-design strategies. The solutions obtained also provide substantial gains in performance with respect to passive design and sequential design strategies. While the results involve open-loop control, the information gained provides important insights into how an implementable system should be designed to achieve enhanced performance, including physical design and control system architecture.

Future work should include a variety of studies, including the investigation of co-design based on fully non-linear rail vehicle models. Investigation of global collocation techniques should be performed to determine whether they offer advantages over local collocation methods. Tradeoff studies between alternative architectures of varying complexities and cost would help generate insights into promising directions for active and semi-active rail suspension systems. More comprehensive test cases should be employed. Future studies should increase the level of model detail and sophistication, working toward practical, realizable designs.

References

[1] Orvnäs, A., 2008. "Active secondary suspension in trains". *Royal Institute of Technology (KTH), Stockholm.*

[2] "Shinkansen 500 train".

[3] Deshmukh, A. P., Herber, D. R., and Allison, J. T., 2015. "Bridging the gap between open-loop and closed-loop control in co-design: A framework for complete optimal plant and control architecture design". In American Control Conference (ACC), 2015, IEEE.

[4] Spencer Jr, B., Dyke, S., Sain, M., and Carlson, J., 1997. "Phenomenological model for magnetorheological dampers". *Journal of engineering mechanics.*

[5] Garg, V. K., and Dukkipati, R. V., 1984. *Dynamics of Railway Vehicle Systems.* Academic Press.

[6] Cheng, Y.-C., Lee, S.-Y., and Chen, H.-H., 2009. "Modeling and nonlinear hunting stability analysis of high-speed railway vehicle moving on curved tracks". *Journal of Sound and Vibration.*

[7] Graa, M., Nejlaoui, M., Houidi, A., Affi, Z., and Romdhane, L., 2016. "Development of a reduced dynamic model for comfort evaluation of rail vehicle systems". *Proceedings of the Institution of Mechanical Engineers, Part K: Journal of Multi-body Dynamics.*

[8] Hirotsu, T., Terada, K., Hiraishi, M., and Shigetomo, Y., 1991. "Simulation of hunting of rail vehicles: The case using a compound circular wheel protile". *JSME international journal. Ser. 3, Vibration, control engineering, engineering for industry.*

[9] Goodall, R., 1997. "Active railway suspensions: Implementation status and technological trends". *Vehicle System Dynamics.*

[10] Orvnäs, A., 2011. "On active secondary suspension in rail vehicles to improve ride comfort". PhD thesis, KTH Royal Institute of Technology.

[11] Goodall, R., and Kortüm, W., 2002. "Mechatronic developments for railway vehicles of the future". *Control Engineering Practice.*

[12] Persson, R., 2008. "Tilting trains: technology, benefits and motion sickness". PhD thesis, KTH.

[13] Suzuki, H., Shiroto, H., and Tezuka, K., 2005. "Effects of low frequency vibration on train motion sickness". *Quarterly Report of RTRI*.

[14] Ashour, O., Rogers, C. A., and Kordonsky, W., 1996. "Magnetorheological fluids: materials, characterization, and devices". *Journal of intelligent material systems and structures*.

[15] Du, H., Sze, K. Y., and Lam, J., 2005. "Semi-active h control of vehicle suspension with magneto-rheological dampers". *Journal of Sound and Vibration*.

[16] He, Y., 2003. *Design of Rail Vehicles with Passive and Active Suspensions Using Multidisciplinary Optimization, Multibody Dynamics, and Genetic Algorthims*. University of Waterloo [Department of Mechanical Engineering].

[17] Wang, D., and Liao, W., 2009. "Semi-active suspension systems for railway vehicles using magnetorheological dampers. part i: system integration and modelling". *Vehicle System Dynamics*.

[18] Wang, D., and Liao, W., 2009. "Semi-active suspension systems for railway vehicles using magnetorheological dampers. part ii: simulation and analysis". *Vehicle System Dynamics*.

[19] Liao, W., and Wang, D., 2003. "Semiactive vibration control of train suspension systems via magnetorheological dampers". *Journal of intelligent material systems and structures*.

[20] Kwak, M. K., Lee, J.-H., Yang, D.-H., and You, W.-H., 2014. "Hardware-in-the-loop simulation experiment for semi-active vibration control of lateral vibrations of railway vehicle by magneto-rheological fluid damper". *Vehicle System Dynamics*.

[21] Graa, M., Nejlaoui, M., Houidi, A., Affi, Z., and Romdhane, L., 2016. "Mechatronic suspension design for full rail vehicle system". *Proceedings of the Institution of Mechanical Engineers, Part K: Journal of Multibody Dynamics*.

[22] Graa, M., Nejlaoui, M., Houidi, A., Affi, Z., and Romdhane, L., 2016. "Mechatronic suspension design for full rail vehicle system". *Proceedings of the Institution of Mechanical Engineers, Part K: Journal of Multibody Dynamics*.

[23] Sharma, S. K., and Kumar, A., 2017. "Ride comfort of a higher speed rail vehicle using a magnetorheological suspension system". *Proceedings of the Institution of Mechanical Engineers, Part K: Journal of Multi-body Dynamics*.

[24] Arora, M., Luan, S., Thurston, D. L., and Allison, J. T., 2017. "Hybrid procedure-based design strategies augmented with optimization". *ASME 2017 International Design Engineering Technical Conferences*, Aug.

[25] Messac, A., 2015. *Optimization in practice with MATLAB®: for engineering students and professionals*. Cambridge University Press.

[26] Allison, J. T., and Herber, D. R., 2014. "Special section on multidisciplinary design optimization: multidisciplinary design optimization of dynamic engineering systems". *AIAA Journal*.

[27] Deshmukh, A., 2013. "Multidisciplinary design optimization of dynamic systems using surrogate modeling approach".

[28] Herber, D. R., 2014. "Dynamic system design optimization of wave energy converters utilizing direct transcription".

[29] Betts, J. T., 2010. *Practical methods for optimal control and estimation using nonlinear programming*. SIAM.

[30] Deshmukh, A. P., 2017. "Optimization and control of wind energy systems for grid integration". PhD thesis, University of Illinois at Urbana-Champaign.

[31] Guo, T., and Allison, J. T., 2017. "On the use of mathematical programs with complementary constraints in combined topological and parametric design of biochemical enzyme networks". *Engineering Optimization*, Feb.

[32] Papalambros, P. Y., and Wilde, D. J., 2000. *Principles of optimal design: modeling and computation*. Cambridge university press.

[33] Tversky, A., and Kahneman, D., 1975. "Judgment under uncertainty: Heuristics and biases". In *Utility, probability, and human decision making*. Springer.

[34] Herber, D. R., and Allison, J. T., 2017. "Nested and simultaneous solution strategies for general combined plant and controller design problems".

[35] Allison, J. T., 2014. "Engineering system co-design with limited plant redesign". *Engineering Optimization*.

[36] Cramer, E. J., Dennis, Jr, J. E., Frank, P. D., Lewis, R. M., and Shubin, G. R., 1994. "Problem formulation for multidisciplinary optimization". *SIAM Journal on Optimization*.

[37] Hedrick, J. K., Wormley, D., Kar, A., Murray, W., and Baum, W., 1979. Performance limits of rail passenger vehicles: Evaluation and optimization. Tech. rep.

[38] Kalker, J. J., 1967. "On the rolling contact of two elastic bodies in the presence of dry friction". PhD thesis, TU Delft, Delft University of Technology.

[39] Lau, Y., and Liao, W., 2005. "Design and analysis of magnetorheological dampers for train suspension". *Proceedings of the Institution of Mechanical Engineers, Part F: Journal of Rail and Rapid Transit*.

[40] Gao, G., and Yang, S., 2006. "Semi-active control performance of railway vehicle suspension featuring magnetorheological dampers". In Industrial Electronics and Applications, 2006 1ST IEEE Conference on, IEEE.

[41] Carter, F., 1928. "On the stability of running of locomotives". In Proceedings of the Royal Society of London A: Mathematical, Physical and Engineering Sciences, The Royal Society.

[42] Allison, J. T., Guo, T., and Han, Z., 2014. "Co-design of an active suspension using simultaneous dynamic optimization". *Journal of Mechanical Design*.

[43] MATLAB Optimization Toolbox, 2017a. Matlab optimization toolbox. MathWorks, Natick, MA, USA.